ORIGIN OF MAJOR AND TRACE PM COMPONENTS IN THE BARCELONA SUBWAY SYSTEM

Oriol Font[1], Teresa Moreno[1], Xavier Querol[1], Vania Martins[1], Daniel Sánchez Rodas[2], Eladio de Miguel[3], Marta Capdevila[3]

(1) Institute of Environmental Assessment and Water Research, IDAEA, CSIC, C/ Jordi Girona 18-24, 08034 Barcelona, Spain.
(2) Center for Research in Sustainable Chemistry-CIQSO. Associated Unit CSIC-University of Huelva "Atmospheric Pollution". Campus El Carmen. University of Huelva, 21071-Huelva, Spain.
(3) Transports Metropolitans de Barcelona, Santa Eulalia, Av. del Metro s/n, L'Hospitalet de Llobregat 08902, Spain.

Corresponding author: oriol.font@idaea.csic.es

ABSTRACT

Wear in train and rail components in the Barcelona Metro system includes brake pads, catenary wires, wheels, rail ways, and motor brushes. These components were characterised to evaluate their contribution to ambient particulate matter (PM) levels in two platforms (conventional F-L3 and new S-L9). The observed chemical compositions of these components were used to interpret the mineralogical, chemical, and leachability patterns of subway platform particulate matter (PM). F-L3 Frontal brake pads are composed of two distinct layers of different composition: a dark layer (carbon, barite ($BaSO_4$), and zincite (ZnO)) and a reddish layer (hematite (Fe_2O_3) and periclase (MgO)). Lateral brake pads are composed of metallic-Fe with dolomite (CaMg ($CaCO_3$), zinzite, portlandite ($Ca(OH)_2$), as well as Sb, Zn, and Mo sulphide species rich in Cu, Ni, Cu, As, Hg, Cd, and Pb. Motor brushes are composed of carbon nano-tubes (95% C). Sparkling of the catenary (98% metallic-Cu) and wheel/rail (98% metallic-Fe) abrasion are the primary sources of As, Hg, Cu, and Sb in PM, and give rise to fine condensed and water-soluble As species (most likely As_2O_3 and As_2O_5). Moreover, the stibnite (Sb_2S_3)-rich lateral brake pads used in L9 also contribute to fine Sb oxides.

Sulphide-rich brake pads significantly increase and change the occurrence mode of the Zn, Cu, Mn, Cr, Pb, and Ni present in PM by oxidation of brake-bearing metal sulphide to relatively water-soluble sulphate and oxide species. Frontal brake pads are the primary source of Ba and Zn in subway platform PM.

Keywords: PM; subway; wear; brake pads; trace elements

HIGHLIGHTS

-Frontal brake pad wear is the primary source of Ba and Zn in PM.

-Lateral brake pad wear is a source of Sb, As, Zn, Mo, Hg, and Pb in PM.

-Steel wear is the main source of As, Hg, Sb, and Mo in platform air PM when frontal brake pads are employed.

-The wear processes raises PM levels and modify the speciation of As, Hg, Sb, Zn, and Cu by oxidation to more water soluble and toxic species in platform air PM.

-The results of the present study highlight the need for substituting conventional friction materials to reduce metal exposure in commuting.

INTRODUCTION

Commuting accounts for a large proportion of daily human exposure to PM (Adams et al., 2001; Gómez-Perales et al., 2007). Underground metro systems are one of the most sustainable and environmentally-friendly forms of public transport, and energetically and environmentally efficient systems such as low emission electric trains can transport a large number of passengers (million/day, Nieuwenhuijsen et al., 2007), thereby reducing traffic congestion on the surface. Incentivising the use of public transport is has been incorporated into air quality plans in European cities as an

effective tool for the abatement of atmospheric emissions from the transport sector in urban agglomerations (Nagl et al., 2007). Nevertheless, poor air quality in metro systems, especially regarding the levels of PM and metals, have been reported in a number of studies (Fromme et al., 1998; Adams et al., 2001a and b; Furuya et al., 2001; Award, 2002; Seaton et al., 2005; Johansson and Johansson, 2003; Karlsson et al., 2005; Aarnio et al.,2005; Cheng et al., 2008; Ye et al., 2010; Cheng and Yan., 2011; Kam et al., 2011; Querol et al., 2012; Moreno et al., 2015a.; Moreno et al., 2015b; Martins, et al., 2015; Martins, et al., 2016; among others). During metro commuting, abrasion, sparking, and resuspension may cause high levels of exposure to PM (Adams et al., 2001a; Chan et al., 2002a and b; Aarnio et al., 2005; Gómez-Perales et al., 2007; Tsai et al., 2008; Querol et al., 2012; Moreno et al., 2017). Major PM emission sources affecting commuting exposure levels in metro systems include: a) Rail/wheel, brake, and catenary wear; b) Resuspension of deposited materials by air turbulence in stations and tunnels; c) PM emissions from night-time maintenance works, including the use of traction fuel oil engines, construction works, and welding dust; d) Cleaning activities; e) Surface air uptake from the surface, usually highly polluted by urban emissions; f) Sporadic flooding and fire episodes; g) Wind erosion by intense air flow within the tunnels and on platforms (Adams et al., 2001a; Chan et al., 2002a and b; Aarnio et al., 2005; Gómez-Perales et al., 2007; Tsai et al., 2008; Salma et al., 2007, Salma, 2009a; Moreno et al., 2017).

Results from existing metro system studies point to steel and catenary fusion as the primary sources for Cr (Salma et al., 2009), Mn (Pfeifer et al., 1999), Fe, and Cu (Furuya et al., 2001). Additional studies (Nieuwenhuijsen et al., 2007; Salma et al., 2007; Kam

et al., 2011; Ho et al., 2012) have concluded that rubber wheel systems cause less PM pollution than steel wheel systems, while electric braking systems produce less PM emissions than conventional brake pads, with newer metro systems usually having lower PM exposure levels due to the implementation of advanced technologies, including improved ventilation systems and platform screen door systems. Further measures to reduce PM levels in platforms include washing railways and tunnel walls (attaining a 13% reduction in the PM2.5 in the Stockholm underground; Johansson and Johansson, 2003), tunnel washing (Salma et al., 2007), clean up and reconstruction (low PM10 in the Prague underground; Branis, 2006), installation of platform screen doors (Ho et al., 2012) and the improvement of ventilation systems and protocols (Querol et al., 2012; Moreno et al., 2017). Platform screen door systems have already been installed in a number of metro systems in US, Canada, Brazil, Japan, Denmark, Seoul, and UK, among others, in order to reduce the number of accidents but also for more effective temperature and ventilation control on platforms. In one Seoul subway station, the PM10 and PM2.5 levels were reduced by approximately 15% after screen door installation (Ho et al., 2012). In the Barcelona Metro system, the installation of screen doors coupled with an advanced ventilation system in new metro lines resulted in a drastic reduction (50-66%) of PM levels with respect old and conventional metro lines (Querol et al., 2012; Moreno et al., 2015a.; Moreno et al., 2015b; Martins, et al., 2015; Martins, et al., 2016; Moreno et al., 2017).

Barcelona Metro includes a total of 11 metro lines absorbing 1.25 million passengers on workdays (approximately 50% of the city's public transport use), with an average commuting time of 35 min (Querol et al., 2012). The different metro lines were built in

1929 and 2010 (new L9 and L10 lines were built in 2010 although the southern branch of line 10 was not in operation since September 2018). The metro includes different station designs, consisting of: a) two platforms in the same tunnel with the two rail tracks in the centre running in parallel, one for each direction; b) two platforms separated by a middle wall or built in different tunnels; c) single platforms in different tunnels with platform screen door systems and advanced ventilation systems (new lines L9 and L10); and d) single narrow tunnel with one rail track and a single tunnel with one rail track separated from the platform by a wall with platform screen doors (Martins et al., 2015). Electric braking is engaged during the approach to the platform, though pneumatic braking (asbestos-free) is employed after deceleration to a certain velocity (10-30km/h). The trains of old lines are equipped with motor brushes and use frontal and lateral brake pads, whereas trains of new lines (L9 and L10) are brushes-free and use lateral brake pads. Most of the metro lines are equipped with a Cu-rich catenary system and graphite-rich pantographs, whereas the L4 line is equipped with a Cu-rich catenary system and pantographs. Metal wear, brake wear, and outdoor air were identified as the major sources of PM in platforms (Querol et al., 2012; Martins et al., 2016). Iron bearing species, mainly hematite (Fe_2O_3), magnetite (Fe_3O_4) and metallic Fe, from nanometres to micrometres in size, are the dominant particle type (36-51% of the PM load) originating from wheel/railway abrasion and the wear of Fe-rich materials throughout the system (Moreno et al., 2017). Metallic Fe is oxidised to magnetic oxide species (magnetite and maghemite) and finally to non-magnetic hematite during abrasion by air and thermal oxidation (Moreno et al., 2017).

PM concentration in the old lines of the Barcelona subway (i.e. L3) is generally higher than in the new lines (Querol et al., 2012; Martins et al., 2015). Apart from an advanced ventilation system and screen doors, the different brake pad compositions of these braking systems may account for much higher levels (by factors from 5 to 200) of specific metals such as Ba, As, Sr, Mo, and Cu, among others, in the conventional L3 line, or Sb in the new L9 line. It is likely that the different friction pattern required for frontal (L3) compared to lateral (100% of trains L9 and 20% of trains in L3) braking accounts for a different brake composition. The performance of brake pads is a complex function of numerous parameters (formulations, temperature, pressure, and environment) and large number of base materials, some of which are of environmental concern, potentially toxic, and commonly used in the brake pad manufacturing (Anderson, 1992; Bijwe, 1997; Weiss et al., 2006; Amato et al., 2012). The most important materials employed in the brake pad manufacture are: a) fibres (glass and aramid fibres, and Rockwool) used to link the other components, being the frame of the brake pads; b) mineral fillers (barite, magnesite, talc, carbonates, feldspars, and micas) to provide mechanical consistency and resistance to abrasion and cuts; c) shavings and powdered metallic components (Fe, Cu, bronze, and brass) to homogenise the friction coefficient and heat transfer throughout the pad; d) lubricants (stibnite (Sb_2S_3), pyrite (FeS_2), sphalerite (ZnS), graphite, and coke) to reduce the friction coefficient; e) organic components (phenolic resins, rubbers, waxes, and oils) to agglutinate the brake pad components by melting and subsequent flowing throughout the friction material of brake pads; and f) abrasives (cubic boron nitride, alumina, feldspars, silicon carbide, and diamond) to increase the friction coefficient and to clean the disk surface of the disk brakes (Nagesh et al., 2014). In addition, brake

pad wear, the abrasion and/or sparking of steel-like materials (such as catenary, wheels, and rails) may also contribute to increased levels of certain elements (As, Cu, Mo, Sb, Pb, Ni, P, and Sn) which are typical components and/or impurities of the steel and catenary. Trains equipped with C motor brushes may contribute to raise the PM levels of elemental carbon (EC), since their wear is remarkable (these are changed once per year; TMB personal communication). Therefore, it can be thought that steel emissions (from wheel and rail abrasion) represent the most important source of PM, although other sources may be significant contributors to the PM emissions of specific trace metals.

The aim of the present study is to determine the origin (e.g. brake pads, catenary, wheels/rail ways, and motor brushes) and speciation of elements of environmental concern (i.e. As, Sb, Zn, Hg) in the ambient air PM of the Barcelona Metro system for assessing subsequent remediation and emission abatement measures.

2. MATERIALS AND METHODS

2.1. Samples

Different brake pads from the L3 (1 lateral and 2 frontal, named L3L and L3F) and L9 (2 lateral brake pads, named L9-LA and L9-LB) lines were supplied by “Transports Metropolitans de Barcelona” (TMB). Lateral (commonly named the composite brake pad) and frontal (composite brake blocks) brake linings showed a different morphology (Figure 1). Most trains of the L3 line (80%) are equipped with frontal brake pads, while all trains of the new L9 line use lateral brake lining materials. A section of brake pads was obtained by using a diamond disk saw. Subsequently, a fraction of 1-2 cm^3

(including the metallic support) was removed (Figure 1). The lateral and friction sections of this 1-2 cm^3 fraction were polished for subsequent textural, morphological, and particle resolved composition analysis. The remaining fraction of the section was crushed and milled for subsequent mineralogical and chemical analysis. As shown in Figure 1, the L3 frontal brake pad shows two clearly differentiated layers (reddish and dark layers) from the metallic support to the friction surface. Individual sections of both dark (D) and reddish (R) layers were crushed and milled for subsequent analysis, while the polished section included both layers (named L3-FD1, L3-FR1, L3-FD2, and L3-FR2). A 107mm^2 cylindrical section of the major catenary type (80% of the catenary for the whole metro lines), shavings produced by train wheels during the wheel turning process, and a sample of motor brushes were also supplied by TMB (Figure 2) alongside data on the chemical composition of the railways (UIC 54A steel type). Catenary wear is produced due to friction with pantographs. The pantographs transmit electricity to the trains, and are made of graphite or Cu/graphite. A total of 24 trains from old lines were also equipped with motor brushes. Brush wear is produced by the continuous friction of the motor brushes with the rotor, and 3000-4000 brushes are consumed per year. Each train is equipped with 108 brushes (16 motors per train with 8 brushes each).

2.2 Analysis

The mineralogy of the aforementioned samples was determined by X-ray powder diffraction (XRD) using a Bruker D8 Advance diffractometer with monochromatic Cu Kα1,2 radiation (λ=1,5405) operated at 40 kV and 40 mA. The primary parallel X-ray beam was generated by a Göbbel mirror, and the scattered beam was analysed by a

Sol-X detector with the following scanning parameters: from 4 at 60° of 2θ, a step size of 0.05°, and a time per step of 3 s. The texture, morphology, and particle resolved composition of the samples was investigated by a Quanta 200 scanning electron microscope equipped with energy-dispersive X-ray analyser (SEM-EDX).

For chemical analysis, samples were acid-digested in duplicate using a two-step digestion method devised by Querol et al. (1995). The resulting solution was then analysed by inductively-coupled plasma atomic-emission spectrometry (ICP-AES, IRIS Advantage TJA Solutions, THERMO) and by inductively-coupled plasma mass spectrometry (ICP-MS, X Series II, THERMO) for 57 major and trace elements, respectively. The international reference material NBS1633b was also digested to determine the accuracy of the analytical and digestion methods. The Hg content of friction materials was determined directly in solid samples using a LECO AMA 254 gold amalgam atomic absorption spectrometer. The content of C, H, and N were determined using a Thermo Finnigan flash 1112 elemental analyser, which uses a combustion-reduction based method with a thermal conductivity detector. The leachable potential of major and trace elements was examined for speciation purposes. Leaching tests were performed using MQ water in an ultrasound bath for 15min with a water/milled sample ratio of 30 L/kg for train and rail wear samples. The pH of leachates was determined using a conventional pH-meter, while the concentrations of major and trace elements were determined using ICP-AES and ICP-MS, respectively.

2.3. Additional data

Data on the mineralogy and chemistry of PM10 and PM2.5 samples collected at two Barcelona Metro platforms (F-L3 and S-L9, from old L3 and new L9 lines, respectively) during July 2011 (Querol et al., 2012) was used to determine the contribution of the aforementioned friction materials in ambient air PM, and to estimate changes in trace element speciation. The PM10 and PM2.5 samples were collected at F-L3 and S-L9 platforms from 5 to 25 July 2011 between 8:30 a.m. and 8:30 p.m. using a MCVPM1025 high volume sampler ($30m^3/h$) equipped with quartz microfibers filters (Palflex). To determine the content of soluble ion leaching, ¼ filter was carried out using 30 mL MQ water in an ultrasound bath for 15 min.

The speciation of As and Sb in selected PM10 and PM2.5 filters collected during the sampling campaign was performed employing an analytical procedure based on liquid extraction of the samples, and analysis of the extracts by high performance liquid chromatography coupled to hydride generation and atomic fluorescence spectrometry (HPLC–HG–AFS). This instrumental coupling has previously been employed for the speciation of As (As(III) and As(V)) in PM10 and PM2.5 samples (Sánchez-Rodas et al., 2007; Sánchez de la Campa et al., 2008; Sánchez de la Campa et al., 2018), as well as for Sb speciation (Sb(III) and Sb(V)) in the same type of sample (Alsioufi et al., 2016; Sánchez-Rodas et al., 2017).

3. RESULTS AND DISCUSSION

3.1. Composition of Metro train brake pads

The mineralogical, morphological, and chemical properties of brake pad samples are depicted in Figures 3-6, Tables 1-2, supplementary material S1-S4

3.1.1. L3 frontal brake pad

As previously mentioned, the frontal brake pads are composed of two clearly differentiated layers (dark and reddish layers; Figures 1, 3, and 4). The textural, mineralogical, and chemical characteristics are similar among the two dark (L3-FD1 and L3-FD2) and reddish (L3-FR1 and L3-FR2) layers. The reddish layers (Figures 3 and 4) are characterised by high periclase (MgO) content, and by minor proportions of barite ($BaSO_4$) and calcite ($CaCO_3$). These components are commonly used as mineral fillers in brake lining materials (Anderson, 1992; Bijwe, 1997). Hematite (Fe_2O_3) and zincite (ZnO) are also present in minor to intermediate proportions, and are employed as an abrasive and lubricant, respectively. Magnesium silicate and Ca-Mg Al-Si species were only detected by SEM, indicating that they largely occur in an amorphous form and give rise (together with C) to the background hump between 15 and 35 theta degrees of the XRD spectra of this layer (Figure 3). The reddish layer is characterised by relatively coarse (50-100 μm) texture. Fe_2O_3 particles embedded in a matrix are largely composed of irregular Ca-Mg Al-Si species of variable size (5-50 μm) and fine Mg-Si species (Figure 4b-c). Furthermore, relatively coarse particles (around 30-40 μm) of MgO and C, as well as fine particles (around 5μm) of zincite/sphalerite (ZnO/ZnS), are also present in the matrix (Figure 4c-d). As a result of this mineral composition, the reddish layer shows high concentrations of C (24-25%) and MgO (14-16%, Table 1), with reduced amounts of Ca, Al, and Fe (5.8-9.4%) and minor proportions of S, Na, K, Ba, Ti, and Mn (0.1-2.0%). Regarding trace elements, there is a notable concentration of Cr (136-203 mg/kg).

Carbon is by far the major component (42-44%) of the L3 frontal brake pads and the only lubricant material employed within the dark layers (Figures 3 and 4e), which is directly in contact with the wheels, thereby serving as the wear layer during braking. The amorphous character of C species other than graphite gives rise to the characteristic increase of the background of the XRD spectra between 15 and 30 theta degrees (Figure 3). Barite (mineral filler) is the main crystalline component of the dark layer, with low occurrence of $CaCO_3$ and quartz (SiO_2). Other mineral fillers (such as Ca-Mg Al-Si species) are also present, though were only detected by SEM, indicating an amorphous occurrence. The texture of the dark layer differs significantly from that of the reddish layer, as shown in Figure 4a. Coarse irregular particles of quartz (100-250 μm) and C (mostly of 200 μm) are surrounded by a matrix composed of particles varying in size (generally <50 μm), including barite (some particles up to 25-30 μm), Ca-Mg Al-Si, and Ca-Mg carbonates (Figure 4e-f). Apart from C, the occurrence of the aforementioned species results in notable concentrations of Ba (4.3-6.4%), S (4.2-4.9%), Mg (5.1-5.3%), Ca (4.0%), and Al (3.4-4.0%), Zn (1.4-1.5%), and Ti (0.2-0.3%) oxides. Regarding other elements, Mo (693-764 mg/kg), and Sr (506-589 mg/kg) show the most noticeable concentrations, indicating the probable presence of molybdenite (MoS_2), which is commonly used as a lubricant in brake linings and the and that of Sr partially replacing Ba in the framewok structure ofbarite.

A chemical comparison between the reddish and dark layers (supplementary material, S-1) indicates that the dark layer is highly enriched by Ba (by a factor of 71) and Mo (26), while the reddish layer is enriched by Eu, Bi, Cd, S ,Zn, C, Co, Sr, Sb, Hf, Rb, and Li

by factors ranging from 1.2 to 6. The reddish layer exhibits enrichment (by factors ranging from 1.3 to 4) by Hg, Fe, Mg, Mn, Na, Ca, Ti, Nb, Sc, Cr, Ta, Al, Sn, Y, Th, REES, Ni, P, K, Be, V, Ga, U, and Pb (Figure 5). Arsenic, W, Cu, and Zr are not comparatively enriched in one of the two layers.

Notably, there is a significant analytically unaccounted mass fraction in L3 frontal brake pads (27-30%) that presumably corresponds to total SiO_2 (not measured in our study due to its loss during sample digestion), including quartz and amorphous silica present in Ca-Mg aluminium-silicates. The possible occurrence of nanoparticles of SiC and/or amorphous matter can be ruled out given that no Si was detected by SEM in C particles.

3.1.2. L3 lateral brake pads

The textural, mineralogical, and chemical composition of L3 lateral brake pads is completely different from that of frontal L3 brake pads. Metallic Fe is major mineral component, while $CaMg(CO_3)_2$, portlandite ($Ca(OH)_2$) (mineral fillers), and ZnO, ZnS, and MoS_2 (lubricants) occur in lower proportions (Figures 3c and 5). Coarse shavings of Fe particles (generally 200-900 µm), and sporadically of Cu, and aggregates of Ca-Mg Al-Si cylinders (approximately 100 µm) are embedded in a matrix primarily composed of fine $CaMg(CO_3)_2$ crystals of variable size, (5-30 µm), fine ZnO crystals (commonly <5 µm), and Al-rich areas surrounding the $CaMg(CO_3)_2$ and ZnO crystals (Figure 5). Ca-Mg Al-Si species are also present, were only detected by SEM due to their amorphous character. As a result of the high occurrence of metallic Fe particles, the concentration of Fe accounted for the high proportions (56% as Fe_2O_3) of any element, while the

proportions of C accounted for 15% (Table 1). The occurrence of ZnO, ZnS, and MoS_2 gives rise to relatively high of ZnO (4.6%), SO_3 (5.8%) and Mo (0.4%) content. The presence of $Ca(OH)_2$ and $CaMg(CO_3)_2$ resulted in Ca and Mg contents of 8.2% and 1.8%, respectively.

3.1.3. L9 lateral brake pads

The lateral brake pads from L9 all resembled similar textural, mineralogical, and chemical properties, with few differences between them. This brake pad type is characterised by a higher occurrence of abrasives and lubricants than mineral fillers. Metallic Fe (abrasive), and stibnite and zincite (lubricants) are the major mineral phases, with a significant occurrence of quartz, hematite, sphalerite, and graphite (Figure 3). Barite and MgO (the later only in L9-2 sample) are the major mineral fillers employed, and these occur in notable proportions, while calcite ($Ca(OH)_2$), and pyrite (FeS_2) are present in trace amounts. Coarse (mostly ~200µm, though up to 600 µm) and generally rounded particles of Fe, sporadic Cu particles (containing Zn, Al, and Fe), and Fe-Al particles are embedded in a matrix primarily consisting of finer particles (<20µm) of Sb_2S_3, $BaSO_4$, C, and FeS_2 (Figure 6a-c). Furthermore, irregular particles of Al and Mg, probably in oxide form, are also present in the matrix (Figure 6b). As a result of this mineral composition, Fe shows the exhibits the concentration (46-47% as Fe_2O_3), followed by C (21-24%), Cu (3.5-9.9%), ZnO (6.5-8.8%), SO_3 (5.7-7.7%), CaO (2.9-3.9%), Mg (3.5-4.3%), BaO (1.6-2.1%%), MnO (0.4%), and Sb (0.3-0.5%) (Table 1).

A comparison of the chemical composition between L3 and L9 brake pads (L9/L3 brake pads concentration ratio) reveals the following enrichment patterns (Table 1 and supplementary material S-2):

a) L9 brake pads are specially enriched in Cu (1245 times higher) and Sb (235) with respect to the entire composition of L3 frontal brake pads (calculated according the corresponding percentage of each layer; 80 and 20% for the dark and reddish layer, respectively).

b) L9 brake pads are also significantly enriched with Ge, Se, Pb, As, Fe, Hg, Zn, Ni, Mn, Co, S, P, Cd, and Cr by a factors ranging from 1.3 to 193 with respect to the entire L3 frontal brake pad.

c) L3 frontal brake pads is enriched (in decreasing order) with Li, Sc, B, Zr, Th, REEs, W, Ta, Hf, Be, Al, U, Ti, Nb, Na, Y, K, Bi, V, Rb, Mo, Mg, Sr, Sn, Ca, C, Ba, and Ga, with respect L9 lateral brake pads by a factors ranging from 1.3 to 1013.

d) L3 lateral brake pads exhibit similar enrichment patterns to L3 frontal brake pads with respect L9 lateral brakes, but with a greater level of Mo, Cd, and Fe enrichment. Strontium, Mg, and C are not enriched in L3 lateral brakes with respect to L9 lateral brakes.

The occurrence of MgO and $Ca(OH)_2$ give rise to the relatively alkaline pH of brake pad leachates (supplementary material S-3). Moreover, the relatively high release of Ca and Mg leachates from both L3 frontal and lateral brake pads shows significant leachable concentrations of Ba, Sr, Mo, and Cu alongside remarkable leachable concentrations of Sb in the L3-FR brake pads. This may be attributed to a rapid saturation and subsequent precipitation of $BaSO_4$ (low soluble mineral) in L3-FD

brakes. The highest leachability of Zn occurs in L3-FD, and significant leachable concentrations of Mo were found in L3-L. The highest leachable concentrations of Sb and As were obtained in the leachates of L9-L brake pads, due to the high occurrence of stibnite (relatively soluble at alkaline pH, giving rise to antimonites complexes; Filella et al., 2002), FeS_2, and ZnS, which may also contain As.

Regarding the mode of occurrence among brake pad elements, Mn, Fe, Zn, Co, Ni, Cu, As, Cd, Sb, W, and Pb are positively correlated with S (r=0-6-0-8) and exhibited negative correlations with Al (R>-0.6), indicating a sulphate/sulphide affinity. Furthermore, As, Hg, Ni, Cu, Cd, and Co are highly and positively correlated with Zn and Sb (r>0.8), indicating a major occurrence of these elements in the framework structure of ZnO/ZnS and Sb_2Sb_3. Moreover, Boron and Se exhibited a positive correlation with C (r=0.9), suggesting a partial organic affinity for these elements.

3.2. Composition of catenary, wheels, railways, and motor brushes

The catenary (Table 2) shows a 99% Cu purity with minor Fe content (0.9%) and trace concentrations of Ti, Zn, Cr, Ni, Sb, Mo, V, Sr, Ba, As, and Hg that remain in trace amounts after the Cu smelting and refining process due to the difficulty of removing them completely during electrolysis (Deeley et al., 2000). Most of these impurities, including those of Cu, Mn, Zn, Sb, Mo, Ba, Sr, and Pb, show low leachable concentrations (Table 4).

The steel of train wheels (Table 2) is composed of 98% metallic Fe with minor amounts of C (0.5%), Mn (0.7%), Cu (0.15%), and Cr (0.12%). Nickel (782 mg/kg), Mo (451

mg/kg), W (91 mg/kg), Sn (95 mg/kg), As (51 mg/kg), Co (80 mg/kg), and Sb (24 mg/kg) attained relatively high concentrations. Most of these elements are present as impurities from Fe ore (ie As), and also due to their addition (primarily Sb, Mo, Cr, and Sn) in the steel manufacturing process to improve its properties (Deeley et al., 2000). Arsenic, Ni, and Cu are commonly present in the structure of ferrite grains of steel (a Fe oxide-like spinel originating when low cooling of molten steel is produced; Smith, 1994). Consequently, steel in the train wheels slowly releases Fe, Mn, Ba, Sb, and Cu when leaching with water (Supplementary Table 4), although the formation of a thin oxide layer on the surface of steel materials limits the release of these trace elements (Deeley et al., 2000). The steel composition of the rails (Table 2) is not significantly different from that of the wheels, also being composed of 98% Fe with minor contents of C (0.7%), Mn (1,1%) and Si (0,3%), and significant concentrations of S (98 mg/kg), P (170mg/kg), Al (11 mg/kg), Ti (16 mg/kg), Cu (158 mg/kg), and Ni (192 mg/kg).

Furthermore, the motor brushes (Table 2) are composed of C nano-tubes (95% C) as deduced from the XRD patterns (pattern 00-058-1638 from the PDF-2 release 2010 International Center of Diffraction Data database), with Zn, Ti, Ba, Sn, and Cr as the main impurities (Table 3). Moreover, leachates of the motor brushes (Table 4) show concentrations below the detection limit for most elements, with the exception of Ca (17 mg/kg), Mn (4.9 mg/kg), and Ba (0.3 mg/kg).

According to the aforementioned mineralogical and chemical composition of train and rail wear, the following patterns of potential major and trace element emission sources in the air of subway systems are highlighted:

a) Wheel/rail steel and the catenary system are the main sources of Fe and Cu within ambient PM on platforms. Lateral brake pads may also represent a significant source.

b) Frontal brake pads may be the most important source of Ba, Zn, and C, and also U, Th, and REEs. These elements (U, Th, and REEs) are found in detectable concentrations in L3 frontal brake pads.

Furthermore, the temperatures reached during braking, sparking, and abrasions may produce the following changes in the mode of occurrence of elements present in wear materials:

a) The temperatures reached during braking may also result in these elements through the oxidation of sulphides to sulphate and oxide species. Stibnite is oxidised to Sb_2O_5, Sb_2O_3, and Sb_2O_4 (Cho et al., 2006), molybdenite to MoO_3 (Cho et al., 2006), ZnS to $ZnSO_4$, $Zn_3O(SO_4)_2$, and ZnO (Shultze et al., 1995), and FeS_2 to Fe_2O_3.

b) Sparking of the catenary may give rise to the volatilisation/condensation processes of specific trace elements such as As, Hg, Sb, and Zn due to the presumed high temperature of sparking, most probably resulting in their condensing as very fine oxidised species that may be adsorbed by Fe particles.

c) The temperatures of the wheels/railway abrasion may result in the fusion/sintering processes of steel, giving rise to rounded Fe- particles and sintered structures, as reported by Querol et al (2012).

3.3. Effect of train and rail wear on the PMx levels of platforms

3.3.1. Enrichment and leachable patterns of major and trace elements in platform airborne PM

As reported in previous studies (Querol et al., 2012; Moreno et al., 2017) the installation of screen doors and advanced ventilation systems, such as in the L9 line, accounts for lower PMx load and lower PMx levels for most elements with respect to those of conventional lines such as L3 (Table 3). Exceptions to this are the elements arising from outdoor air (i.e. Cl^-, NO_3^-, SO_4^{2-}, NH_4^+, Se, and V; Querol et al., 2012; Martins et al., 2015) and ballast components (i.e. Ca, K, Na, P, U, Th, Ta and REEs elements) with higher levels in PM2.5 from S-L9 than in PM2.5 from F-L3). F-L3 is characterised by higher levels (factors ranging from 5 to 200) of specific metals such as Ba, As, Sr, Mo, and Cu, among others (Table 3).

According to previous studies (Querol et al., 2012: Moreno et al., 2015b) the mechanical wear of steel at the brake–wheel and wheel–rail interfaces mainly give rise give rise to magnetic metallic flakes and splinters in the form of Fe-rich particles (Figure 7a), accounting for 42-41% (as Fe_2O_3) of the F-L3 PM10 and PM2.5 load, respectively, and for 31-51% for S-L9 PM10 and PM2.5 load, respectively, in S-L9. The Fe flake particles undergo progressive atmospheric oxidation from metallic iron to nanocrystals (10–20 nm) of magnetite and maghemite, and in extensive alteration, to more rounded aggregates of non-magnetic hematite nanocrystals (Moreno et al., 2015b). Fine (<2.5µm) rounded particles arising from the fusion/sintering processes of the catenary system and steel—and their subsequent condensation—are abundant in

in F-L3 PM (Figure 7b) originating from sparking of the catenary and fusion/sintering processes during wheel/railway abrasion. Brake pad wear gives rise to ultrafine (peaking at 0.28 and 0.35 μm diameter), fine (0.6 μm), and intermediate (3-6μm) speed/temperature-dependent particles (Abassi et al., 2012; Iijima et al., 2007). Temperature dependence in the generation of ultrafine particles is especially relevant for 0.28 μm particles (Abassi et al., 2012). The studies conducted by Iijima et al. (2007) indicate that most Sb and other brake pad-bearing elements are 3-6μm in size. According to the aforementioned studies, discrete barite particles (<5μm) and very fine (<2μm) barite and Cu particles onto rough-Fe particles arising from brake pad wear were identified in S-L9 PM (Figures 7c and d).

To withdraw the previously mentioned effect of platform design on PM load and on their enrichment in PM10 or PM2.5, and elucidate properly the former wear component from which a given element is released to the ambient air PM in platforms (F-L3 and S-L9), the concentrations of elements were weight-normalised (wn) dividing the PM10 and PM2.5 levels of each element by the corresponding PMx load (PM10 and PM2.5)of the filter (Table 4). Subsequently the wn PM10/PM2,5 ratios were calculated to determine the enrichment of elements in the PM fractions. Elements with wn-PM10/wn-PM2.5 ratios≥1.2 were considered enriched in PM10, while those with wn-PM10/wn-PM2.5 ratios≤0.8 were considered enriched in PM2.5, and those with ratios 0.8≤wn-PM10/wn-PM2.5≤1.2 were not considered enriched.

The following wnPM10/wnPM2.5 enrichment patterns were obtained for F-L3 platform PMx weight normalised values (Table 4):

a) Elements enriched in PM10 (wn-PM10/wn-PM2.5>1.2): water soluble (ws)-NO_3^-, SO_4^{2-}, Ca, Cu, K, Ti, P, Bi, and Se.

b) Elements enriched in PM2.5 (wn-PM10/wn-PM2.5<0.8): Hg, Sb, As, W, Hf, Ge, U, Ta, and REEs.

c) Elements not enriched in PM10 or PM2.5 (0.8≤ wn-PM10/wn-PM2.5 ≤1.2):ws-Cl^-,ws-SO_4^{2-},ws-NH_4^+,CO_3^{2-}, Al, Ba, Mg, Mn, Zn, Na, Cr, Sr, Mo, Sn, Ni, V, Li, Rb, Nb, Ga, Y, Th, Cd, Pr, and Nd.

The following wn-PM10/wn-PM2.5 enrichment patterns were obtained for S-L9 platform PMx weight normalised values (Table 4):

d) Elements enriched in PM10 (wn-PM10/wn-PM2.5>1.2): ws-NO_3^-, SO_4^{2-}, ws-SO_4^{2-}, SO_4^{2-}, CO_3^{2-}, Ca, Al, Ba, Mg, Zn, Na, K, Ti, Sr, As, Sb, V, Li, Rb, Nb, Se, and REEs.

e) Elements enriched in PM2.5 (wn-PM10/wn-PM2.5<0.8): Cu, Zr, Sb, Ni, Ge, U, Y, and Th.

f) Elements not enriched in PM10 or PM2.5 (0.8<wn-PM10/wn-PM2.5<1.2): OC+EC, ws-Cl^-, MnO, Cr, Hg, Mo, Sn, Co, P , W, Hf, Ga, Ta, Cd, Bi, and Sm.

As may be deduced from the aforementioned enrichment patterns, most of the elements enriched in PM10 and those not enriched in PM10 and PM2.5 arise from outdoor air sources or are of crustal origin (e.g. calcite, illite, and chlinoclore were detected in the PM2.5-10 fraction of F-L3 and S-L9; Querol et al., 2012). Furthermore, elements arising from the wear of friction materials may be enriched either in PM10 or PM2.5, depending on the friction material (e.g. brakes, catenary system, and wheels/railways) and wear type.

The leachates of PM10 and PM2.5 samples from F-L3 and S-L9 platforms (Table 5) exhibit a near neutral pH (6.8-7.3) and contain relatively high and variable concentrations (largely between 0.1 and 3.0 μg/m^3) of Cl^-, NO_3^-, SO_4^{2-},NH_4^+, Ca, Fe, K, Mg, Na, and Ba, with trace and variable concentrations of Li, B, Sc Ti, V, Cr, Mn, Ni, Cu, Zn, As, Se, Sr, Mo, Sb, and Pb (Table 5). With the exception of Cr, Ni, and Zn, the leachable potential of the elements show a positive correlation (R^2=0.7-0.9) with their bulk levels in platforms. As such, the leachable levels of Fe, K, Mg, S, Li, B, Sc, Ti, Sc, Mn, Cu, As, Rb, Sr, Mo, Sb, and Ba are higher in F-L3 than in S-L9, while those of S, V, Se, and Na are similar between F-L3 and S-L9, whereas the leachability of Cr, Ni, and Zn is higher in S-L9 than in F-L3.

The source, enrichment patterns (PM10/PM2.5 weight normalised partitioning), and speciation for a number of elements of environmental concern are described in detail within the following section (Figures 8a and b).

3.3.2. Arsenic

The enrichment and leachability patterns of As are completely different between F-L3 and S-L9 platforms (Figure 8a), suggesting a different speciation for this element between the two subway lines. In the F-L3 platform, As is enriched in the PM2.5 (54%) and displays a high water-soluble proportion in both PM2.5 (63%) and PM10 (54%, Figure 10a). The speciation procedure of As in the F-L3 platform yielded lower As extraction yields (10-22% for PM10 and 8-37% for PM 2.5) than those obtained when leaching the filters using pure water (54-63%). Such low As extraction yields are attributed to the adsorption of As by Fe species (main components of the wear

materials) at the acidic pH of the extraction (3-4) used for As speciation. Consequently, the proportions of As (III) and As (V) obtained are under evaluation, and thus not representative. In spite of this As adsorption process, the presence of both As (III) and As (V) in the extraction solutions confirms the oxidation of elemental As from steel (where it is present as ferrite or/and elemental As, and is the main source of As in S-L3). These features suggest that As is released from ferrite grains included in the steel, from catenary system due to abrasion temperatures during braking, and to the sparking of the catenary system and pantographs, respectively. The fusion of the steel generates fine rounded particles of Fe-C (Figure 7b) that most probably contain oxidized As from ferrite grains. The high temperature of sparking gives rise to the volatilisation/condensation processes of As, leading to finely condensed and highly water-soluble As species. The high water leachability potential of As in F-L3 and in speciation studies indicates the occurrence of highly soluble and harmful As_2O_3 and As_2O_5, which are the primary products of elemental As and As sulphide oxidation. The increased temperature experienced during braking may also produce these As particles, which are mainly released from steel due to the abrasion between wheels and rails, as well as from brakes following the thermal oxidation of As-bearing sulphides. The PM10 fraction of As corresponds to the As included in the laminar hematite particles arising from wheel/rail wear.

In the S-L9 platform, As is highly enriched in PM10 (66%), with very low water leachable proportions (≤5%) in both PM10 and PM2.5. The speciation test showed extraction yields ranging from 18 to 97% (Table 6)—much higher yields than those obtained for pure water, which reveals a high proportion of As (III) with respect to As

(V) in both PM2.5 (60-40% As III) and PM10 (55-45%) (Table 6). These features of the S-L9 platform—particularly the low water extraction yields and the prevalence of As (III) over As(V) in both PM10 and PM2.5—indicate that the wear of sulphide-bearing As species from brake pads is the main origin of this element in platform air PM, with a low occurrence of volatilisation/condensation processes from steel fusion (rounded fusion particles were not detected in S-L9).

3.3.2. Antimony

Antimony shows similar enrichment and leachability patterns between F-L3 and S-L9 PM (Figure 8a), which are largely enriched in PM2.5 (60 and 69% in F-L3 and S-L9, respectively) with relatively high leachable proportions in PM10 (around 20%) and lower leachable proportions in PM2.5 (16 and 7% for F-L3 and S-L9, respectively). Conversely, the speciation of Sb is relatively different between F-L3 and S-L9 airborne particles. Complete antimony occurs as Sb (V) in F-L3 (Table 6), whereas significant proportions (20-39%) of Sb(III) are present in S-L9. The relatively high leachable proportions in PM10 and PM2.5 from F-L3 and in PM2.5 from S-L9 PM10, as well as the high occurrence of Sb (V) in the airborne particles from both platforms, provides evidence of the oxidation of Sb species from friction materials during wear processes.

It can be concluded that steel is the primary source of Sb in the airborne particles, which is oxidised to Sb(V) (most likely Sb_2O_5), whereas the use of stibnite-rich brake pads in trains from the L9 line gives rise to the significant proportions of unaltered Sb (III) in airborne particles. The occurrence of Sb(V) in ambient air particles in S-L9 platform arises from stibnite oxidation during braking and subsequent steel abrasion.

Stibnite oxidises to Sb_2O_5 and Sb_2O_3 at 300-430^oC and to Sb_2O_4 at 570^oC (Cho et al., 2006). Thermal oxidation of metallic-Sb (present in steel and in catenary systems bearing Cu) also gives rise to Sb_2O_3 (Cho et al., 2006). Both Sb_2O_3 and Sb_2O_4 are insoluble or of extremely low solubility, whereas Sb_2O_5 is relatively water soluble (0.003 g/L; Haynes et al., 2014).

3.3.3. Mercury

Mercury follows a similar enrichment and leachability pattern to that of As and Sb in F-L3 and S-L9, respectively. This element reaches higher proportions in PM2.5 than in PM10 in F-L3 (57%), and extremely high leachable fractions in PM2.5 (90%); whereas in PM10, the insoluble Hg species prevails (90%, Figure 8a). The PM2.5 fraction of Hg is produced by the volatilisation and thermal oxidation of Hg, and the subsequent condensation caused by catenary sparking. The high leachability of Hg suggests the occurrence of relatively soluble HgOH (Harris, 1995) that may arise from the hydrolysis of HgO by the subway air moisture. The oxidation of Hg present in brake pads may also contribute to the enrichment of this metal and to the occurrence of highly soluble Hg species in PM2.5. Moreover, the low leachable fraction in PM10 may be due to the oxidation of sulphide bearing-Hg from brake pads. In S-L9, Hg is similarly enriched between PM10 (49%) and PM2.5 (51%), with relatively high leachability in PM10 and low leachability in PM10. These enrichment and leachability patterns are attributed to the thermal oxidation of stibnite in L9 lateral brake pads, as stated for Sb.

3.3.4. Barium and Zinc

Barium and Zn occur mainly as barite and zinzite/sphalerite in F-L3 and S-L9 brake pads, respectively. Both are enriched in PM10 in F-L3 and S-L9 with relatively higher leachability levels in S-L9 (Figure 8a). The higher leachability of Zn in S-L9 is most probably due to the oxidation of low water soluble sphalerite to the more water soluble zinc-sulphate (0.6 g/L; Anderson, 1992) during braking. The thermal oxidation of sphalerite gives rise to $ZnSO_4$ and $Zn_3O(SO_4)_2$ at low temperatures, giving rise to ZnO as temperature increases (Shultze et al., 1995). Zinzite exhibits extremely low solubility in water. The low leachability of Ba in F-L3 PM may be due to rapid saturation and precipitation in the leachates due to the low solubility of barite (0.0000031 g/L; Haynes et al., 2014).

3.3.5. Molybdenum

Molybdenum is slightly enriched in PM2.5 in both platforms (Figure 8b), with higher leachability potential (approximately 20%) in F-L3 PM than in S-L9 PM (4% and 11% for PM10 and PM2.5, respectively). The enrichment in PM2.5 and the relatively high leachability potential suggests the occurrence of MoO_3 in PM, primarily arising from the oxidation of MoS_2 from brake pads subsequently condensates as fine particles (<2.5µm). Metallic Mo is oxidised to MoO_3 at 800^{o}C and MoS_2 at approximately 700^{o}C (Cho et al., 2006), and it is slightly soluble in water (0.0014g/L; Haynes et al., 2014). The volatilisation of Mo from steel by sparking processes may also contribute to the occurrence of Mo in the PM2.5.

3.3.6. Manganese, Chromium, Copper, and Nickel

These elements follow similar enrichment and leachability patterns between F-L3 and S-L9 PM, with all being enriched in PM10 at F-L3 and in PM2.5 at S-L9, with slightly higher leachable proportions in S-L9 PM—especially in PM2.5 (Figure 8b). The aforementioned patterns indicate that most of the Mn, Cr, Cu, and Ni arise from steel and catenary system wear in F-L3, and from lateral brake pad wear in S-L9, which produces finer particles than steel wear. Cooper, Mn, Cr, and Ni occur partially in the framework of sulphide species (sphalerite and pyrite), being oxidised to more soluble Mn-Cr-Cu-Ni sulphates (63.7, 64, 22, and 40.4 g/L respectively; Haynes et al., 2014), as described for Zn during braking.

These results highlight that, apart from the emission of original components from friction materials that may be of health concern such as Sb_2S_3 or MoS_2 (which also may produce H_2SO_4 under humid conditions; Cho et al., 2006), sparking of the catenary system, steel abrasion, and the wear of sulphide-rich brake pads modify the mode of occurrence and speciation of a number of elements, thus emitting fine, condensed, and relatively water soluble and harmful species of As, Hg, Sb, Mo, Zn, Cu, Cr, Pb, and Mn.

4. CONCLUSIONS

The emission of abrasion products from train and rail wear in the Barcelona Metro subway system significantly contributes to increased ambient concentrations of elements of environmental concern, such as Sb, As, Hg, Cr, Ba, Cu, Pb, and Zn. Frontal and lateral brake pads differ largely in their textural, mineral, and chemical

composition. Furthermore, carbon, barite, and zinzite are the major components of the wear layer of frontal brake pads, with the potential emission of Ba and Zn. Lateral brake pads contain coarse metallic Fe as well as Cu embedded in a matrix of fine particles of stibnite, barite, periclase, graphite, zincite, calcite, portlandite, pyrite, and molybdenite. The high occurrence of sulphide species rich in elements such as Sb, As, Zn, Mo, Hg, and Pb make this wear material an important potential source of these elements in subway platforms. The catenary (99% metallic Cu) and wheel/rail steel (98% metallic-Fe) also contains a large number of additional components, namely Zn, Cr, Ni, Sb, Mo, Sr, Ba, As, and Hg in the catenary system as well as C, Mn, Cu, Cr, Ni, Mo W, Sn, As, Sb, and Hg in wheels/railways also being a potential emission source of these elements in subway platforms, while motor brushes (95% carbon nano-tubes) may represent an important source of C in subway transport systems.

Combining the geochemical results from the enrichment and leachability patterns, it may be deduced that catenary sparking is the main source of As, Cu, and Sb in F-L3, giving rise to fine, condensed, and water soluble As species (most probably As_2O_3 and As_2O_5).

It can be concluded that steel is the primary source of Sb in airborne particles, which is completely oxidised to Sb(V)—most probably (Sb_2O_5)—in F-L3, whereas stibnite-rich lateral L9 brake pads are the main source of this element in S-L9 (20-39% of Sb remains as Sb(III) in platform airborne particles), which gives rise to oxidation to Sb(V) (61-80%) following abrasion processes during braking. The steel contained in wheels and rails significantly contributes to increased PM levels of Fe, Cr, Mn, Ni, and Mo. Sulphide-rich

brake pads (such as the lateral brake pads) significantly contribute to the increased and altered mode of occurrence of the aforementioned elements in PM through the oxidation of brake-bearing metal sulphide to relatively water-soluble sulphate species. Frontal brake pads are the major source of Ba and Zn in PM.

The results of the present study highlight the relevance of metallic catenary and brake pad materials in raising the PM levels of a number of environmentally relevant elements such as As, Hg, Sb, Zn, and Cu, and in the modification of their speciation to a far more soluble and toxic mode of occurrence in PM. These important changes in the mode of occurrence and speciation of elements in the PM of metro platforms points to the need for in-depth PM speciation studies, as well as the need for substituting conventional friction materials with low-metal materials—such as graphite pantographs/catenaries and rubber wheels—to reduce exposure to metals during metro commuting.

ACKNOWLEDGEMENTS

This work was supported by the Spanish Ministry of Economy and Competitiveness, and FEDER funds within the I + D Project CGL2012-33066 (METRO) and the IMPROVE LIFE project (LIFE13 ENV/ES/ 000263). Support is also acknowledged to Generalitat de Catalunya 2014 SGR33.

REFERENCES

Aarnio, P., Yli-Tuomi, T., Kousa, A., Makela, T., Hirsikko, A., Hammeri, K., Raisanen, M., Hillamo, R., Koskentalo, T., and Jantunen, M. 2005. The concentrations and composition of and exposure to fine particles (PM2.5) in the Helsinki subway system, Atmospheric Environment, 39, 5059–5066.

Abbasi, S., Olander, L., Larsson, C., Olofsson, U., Jansson, A., and Sellgren, U. 2012. A field test study of airborne wear particles from a running regional train. Published in IMechE, Part F: Journal of Rail and Rapid Transit, 226, 95–109.

Adams, H. S., Nieuwenhuijsen, M. J., Colvile, R. N., McMulle, M. A., and Khandelwal, P. 2001a. Fine particle (PM2.5) personal exposure levels in transport microenvironments, London UK, Science of the Total Environment, 279, 29–44.

Adams, H. S., Nieuwenhuijsen, M. J., and Colvile, R. N. 2001b. Determinants of fine particle (PM2.5) personal exposure levels in transport microenvironments, London, UK, Atmospheric Environment, 35, 4557–4566.

Akihiro Iijimaa, Keiichi Satob, Kiyoko Yanoc, Hiroshi Tagoa, Masahiko Katoa, Hirokazu Kimurad, and Naoki Furutab. (2007). Particle size and composition distribution analysis of automotive brake abrasion dusts for the evaluation of antimony sources of airborne particulate matter, Atmospheric Environment, 41, 4908–4919.

Alsioufi, A., Sánchez de la Campa, A.M., and Sánchez-Rodas, D. 2016. Microwave extraction as an alternative to ultrasound probe for antimony speciation in airborne particulate matter. Microchemical Journal, 124, 256–260.

Amato, F., Font, O., Moreno, N., Alastuey, A., and Querol, X. 2012. Mineralogy and Elemental Composition of Brake Pads of Common Use in Spain. MACLA, 16, 144–145.

Anderson, A.E. 1992. Friction and wear of automotive brakes.. In: Blau P, editor. ASM handbook. Friction, lubrication, and wear technology, vol. 18. ASM International; p. 569–77.

Award, A. H. A. 2002. Environmental Study in subway metro stations in Cairo, Egypt, Journal of Occupational and Health, 44, 112–118.

Bijwe J. 1997. Composites as friction materials: recent developments in non-asbestos fiber reinforced friction materials-A review. Polymer Composites, 18, 378–96.

Branis, M. 2006. The contribution of ambient sources to particulate pollution in spaces and trains of the Prague underground transport system, Atmos. Environ., 40, 348–356.

Chan, L. Y., Lau, W. L., Lee, S. C., and Chan, C. Y. 2002a. Commuter exposure to particulate matter in public transportation modes in Hong Kong, Atmospheric Environment, 36, 3363–3373.

Chan, L. Y., Lau, W. L., Zou, S. C., Cao, Z. X., and Lai, S. C. 2002b. Exposure level of carbon monoxide and respirable suspended particulate in public transportation modes while commuting in urban area of Guangzhou, China. Atmospheric Environment, 36, 5831–5840.

Cheng, Y. H., and Yan, J. W. 2011. Comparisons of particulate matter, CO, and CO2 levels in underground and ground-level stations in the Taipei mass rapid transit system, Atmospheric Environment, 45, 4882–4891.

Cheng, Y. H., Lin, Y. L., and Liu, C. C. 2008. Levels of PM10 and PM2.5 in Taipei rapid transit system, Atmospheric Environment. 42, 7242–7249.

Deeley, P.D., Kundig, K.J.A., and Spendelow, H.R. Jr. 2000. Ferroalloys & Alloying Additives Handbook. AMG Vanadium, Inc.,60790 Southgate Road, Cambridge, OH, USA.

Filella, M., Belzile, N., Chen, Y-W., 2002. Antimony in the environment: a review focused on natural waters II. Relevat solution chemistry. Earth Sciences Reviews, 59, 265–285.

Fromme, H., Oddoy, A., Piloty, M., Krause, M., and Lahrz, T. 1998. Polycyclic aromatic hydrocarbons (PAH) and diesel Engine emission (elemental carbon) inside a car and a subway train. Science of the Total Environment, 217, 165–173.

Furuya, K., Kudo, Y., Okinagua, K., Yamuki, M., Takahashi, K., Araki, Y., and Hisamatsu, Y. 2001. Seasonal variation and their characterization of suspended particulate matter in the air of subway stations, Journal of Trace Microprobe T., 19, 469–485.

Gómez-Perales, J. E., Colvile, R. N., Fernandez-Bremauntz, A. A., Gutierrez-Avedoy, V., Paramo-Figueroa, V. H., Blanco-Jimenez, S., Bueno-Lopez, E., Bernabe-Cabanillas, R., Mandujano, F., Hidalgo-Navarro, M., and Nieuwenhuijsen, M. J. 2007. Bus, minibus, metro inter-comparison of commuters' exposure to air pollution in Mexico City, Atmospheric Environment, 41, 890–901.

Haynes, W. M. 2014. Handbook of Chemistry and Physics. 95th edition. CRSnetBase, Taylor and Francis Group, LLC. 2014-2015 online version, http://www.hbcpnetbase.com/.

Harris, D.C. 1995. Quantitative chemical analysis. $th Edition. Freeman and Company. USA. pp AP16–20.

Ho, D. X., Jeon, J. S., Kim, J. C., and Kim, K. H. 2012. A noticeable shift in particulate matter levels after platform screen door installation in a Korean subway station, Atmospheric Environment, 49, 219–223.

Johansson, C., and Johansson, P. A. 2003. Particulate matter in the underground of Stockholm, Atmospheric Environment, 37, 3–9.

Kam, W., Cheung, K., Daher, N., and Sioutas, C. 2011. Particulate matter (PM) concentrations in underground and ground-level rail systems of the Los Angeles Metro, Atmospheric Environment, 45, 1506–1516, 2011.

Karlsson, H., Nilsson, L., and Moller, L. 2005. Subway particles are more genotoxic than street particles and induce oxidative stress in cultured human lung cells, Chem. Res. Toxicol., 18, 19–23.

Martins, V., Moreno, T., Minguillón, M.C., Amato, F., DeMiguel, E., Capdevila, M., and Querol, X. 2015. Exposure to airborne particulate matter in the subway system. Sci. Total Environ, 511, 711–722.

Martins, V., Moreno, T., Mendes, L., Eleftheriadis, K., Diapouli, E., Alves, C., Duarte, M., DeMiguel, E., Capdevila, M., Querol, X., and Minguillón, M.C. 2016. Factors controlling air quality in different European subway systems. Environ. Res. 146, 35–46.

Min Hyung Cho, Jeong Ju, Seong Jin Kima, and Ho Jang. 2006. Tribological properties of solid lubricants (graphite, Sb2S3, MoS2) for automotive brake friction materials, Wear, 260, 855–860.

Moreno, T., Reche, C., Rivas, I., Minguillón, M.C., Martins, V., Vargas, C., Buonano, G., Parga, J., Pandolfi, M., Brines, M., Ealo, M., Fonseca, A.M., Amato, F., Sosa, G., Capdevila, M., de Miguel, E., Querol, X., and Gibbons, W. 2015a. Urban air quality comparison for bus, tram, subway and pedestrian commutes in Barcelona. Environ. Res. 142, 495–510.

Moreno, T., Martins, V., Querol, X., Jones, T., BéruBé, K., Minguillón, M.C., Amato, F.,Capdevila, M., de Miguel, E., Centelles, S., and Gibbons, W. 2015b. A new look at inhalable metalliferous airborne particles on rail subway platforms. Sci. Total Environ. 505, 367–375.

Moreno, T., Reche, C., Minguillón, M.C., Capdevila, M., de Miguel, E., and Querol, X. 2017. The effect of ventilation protocols on airborne particulate matter in subway systems. Science of the Total Environment, 584–585, 1317–1323.

Nagesh, S.N., Siddaraju C., Prakash, S.V., and Ramesh M.R. 2014. Characterisation of brake pads by variation in composition of friction materials. Procedia Materials Science ,5, 295 – 302, 2211–8128.

Nagl, C., Moosmann, L., and Schneider, J. 2007. Assessment of plans and programs reported ulder 1996/62/EC – final report, Service contract to the European Commission, DG Environment Contract No. 070402/2005/421167/MAR/C1, REPORT REP-0079, Viena, Umweltbundesamt GMBH, ISBN: 3-85457-876-8, 139pp.

Nieuwenhuijsen, M. J., Gómez-Perales, J. E., and Colvile, R. N. 2007. Levels of particulate air pollution, its elemental composition, determinants and health effects in metro systems, Atmos. Environ., 41, 7995–8006.

Pfeifer, G.D., Harrison, R.M., Lynama, D.R. 1999. Personal exposures to airborne metals in London taxi drivers and office workers in 1995 and 1996. Scienc. Tot. Environ. 235, 253–260.

Querol, X, Fernandez-Turiel, J.L., and López-Soler, A. 1995. Trace elements in coal and their behaviour during combustion in a large power station. Fuel, 74 (3), 331–343.

Querol, X., Moreno, T., Karanasiou, A., Reche, C., Alastuey, A., Viana, M., Font, O., Gil J., de Miguel, E., and Capdevila, M. 2012. Variability of levels and composition of PM 10 and PM 2.5 in the Barcelona Metro system. Atmospheric Chemistry and Physics, 12, 5055–5076.

Salma, I., Pósfai, M., Kovács, K., Kuzmann, E., Homonnay, Z., and Posta, J. 2009a. Properties and sources of individual particles and some chemical species in the aerosol of a metropolitan underground railway station. Atmospheric Environment, 43, 22–23, 3460–3466.

Salma, I., Weidinger, T., and Maenhaut, W. 2007. Time-resolved mass concentration, composition and sources of aerosol particles in a metropolitan underground railway station, Atmospheric Environment, 41, 8391–8405.

Sánchez de la Campa, A.M., de la Rosa, J.D., Sánchez-Rodas, D., Oliveira, V., Alastuey, A., Querol, X., and Gómez-Ariza, J.L. 2008. Arsenic speciation study of PM2.5 in an urban area near a copper smelter, Atmospheric Environment 42, 6487–6495.

Sánchez de la Campa, A.M., Sánchez-Rodas, D., Alsioufi, L., Alastuey, A., Querol, X, and de la Rosa, J.D. 2018. Air quality trends in an industrialised area of SW Spain. Journal of Cleaner Production, 186, 465–472.

Sánchez-Rodas, D., Sánchez de la Campa, A.M., de la Rosa, J.D., Oliveira, V., Gómez Ariza, J.L, Querol, X., and Alastuey, A. 2007. Arsenic speciation of atmospheric particulate matter (PM10) in an industrialised urban site in southwestern Spain, Chemosphere, 66, 1485–1493.

Sánchez-Rodas, D., Alsioufi, L., Sánchez de la Campa, A.M., and González-Castanedo, Y. 2017. Antimony speciation as geochemical tracer for anthropogenic emissions of atmospheric particulate matter. Journal of Hazardous Materials, 324, 213–220.

Schultze D., Steinike, U., Kussin, J., and Kretzschmar U. 1995. Thermal Oxidation of ZnS Modifications Sphalerite and Wurtzite. Crystal Research and Technology, 30 (4), 553–558.

Seaton, A., Cherrie, J., Dennekamp, M., Donalson, K., Hurley, F., and Tran, L. 2005. The London underground: dust and hazards to health. Occupational Environmental Medicine, 62, 355–362.

Smith, E.H. 2013. Technology & Engineering. Mechanical Engineer's Reference Book. 12th edition. Butterworth Heinemann Ltd. Linacre House Jordan Hill, Oxford.

Tsai, D.H., Wu, Y.H., and Chan, C.C. 2008. Comparisons of commuter's exposure to particulate matters while using different transportation modes. Science of the Total Environment, 405, 1–3, 71–77.

Weiss Z., Crelling, J.C., Martynkova, G.S., Valaskova, M., Filip, P. 2006. Identification of carbon forms and other phases in automotive brake composites using multiple analytical techniques. Carbon, 44 (4), 792–798.

Ye, X., Lian, Z., Jiang, C., Zhou, Z., and Chen, H. 2010. Investigation of indoor environmental quality in Shanghai metro stations, China. Environmental Monitoring Assessment, 167, 643–651.

Table 1. Concentrations of major and trace elements in frontal and lateral brake pads from Barcelona Metro lines 3 (L3) and 9 (L9). (L3-FD: frontal dark layer; L3-FR: frontal reddish layer; L3-L: lateral brake pads from L3; L9-L: lateral brake pads from L9). *Calculated.

%	L3-FD1	L3-FR1	L3-FD2	L3-FR2	*whole FL3	L3-L	L9-L1	L9-L2
C	44	24	42	25	37	15	21	24
H	2.5	2.5	2.5	2.3	2.4	1.5	1.8	2.5
N	0.7	1.4	0.7	1.3	0.9	0.3	0.3	0.2
Al_2O_3	4.1	8.8	3.4	6.8	5.6	2.0	0.0	0.1
CaO	4.0	9.4	4.0	8.5	5.8	8.2	2.9	3.9
Fe_2O_3	1.5	6.1	1.5	5.8	3.0	56	46	47
K_2O	0.2	0.4	0.3	0.3	0.3	0.0	0.01	0.01
MgO	5.3	16	5.1	14	8.6	1.8	3.5	4.3
MnO	0.1	0.2	0.1	0.2	0.1	0.3	0.4	0.4
Na_2O	0.5	1.1	0.4	0.9	0.7	0.2	0.03	<0.01
P_2O_5	0.1	0.2	<0.01	0.1	0.1	0.01	0.4	<0.01
SO_3	4.2	1.6	4.9	2.0	3.3	5.8	5.7	7.7
TiO_2	0.3	0.6	0.2	0.4	0.4	0.1	0.003	0.01
BaO	4.3	0.1	6.4	1.1	2.9	0.0	2.1	1.6
ZnO	1.5	0.7	1.4	0.7	1.2	4.6	8.8	6.5
mg/kg								
Li	10.8	9.2	8.9	8.7	10.1	1.7	<0.01	<0.01
Be	0.9	1.6	0.8	1.4	1.1	0.0	<0.01	<0.01
B	<0.01	17	40	25	5.6	16.1	<0.01	<0.01
Sc	4.2	9.4	3.5	8.3	5.9	1.3	<0.01	<0.01
V	43	69	32	66	51	22	4.5	2.2
Cr	91	203	62	136	127	122	204	132
Co	11	6.3	8.5	7.6	9.1	25.9	23.4	14.5
Ni	13	26	8.8	24.9	17.4	67.0	118	104
Cu	56	53	41.2	168.6	54.3	238.3	99711	35436
Ga	3.7	5.8	2.9	5.9	4.3	4.5	3.8	2.5
Ge	0.01	0.01	0.01	0.01	0.0	2.1	1.9	1.9
As	1.6	1.6	1.7	2.0	1.6	12	44	22
Se	0.01	0.01	5.6	2.6	0.0	1.4	2.0	1.1
Rb	9.9	8.3	8.6	8.8	9.3	2.2	1.0	0.8
Sr	589	382	506	380	515	92	189	295
Y	9.5	19.3	8.3	16.9	13	3.8	0.8	0.0
Zr	78.1	69.5	30.1	68.9	74	17	0.01	0.5
Nb	10	24	6.8	20.3	15	3.5	0.5	0.0
Mo	764	29	692	107	514	3631	88	46
Cd	0.9	0.2	0.9	0.0	0.6	3.1	0.5	1.7
Sn	20	43	9	15	28	19	11.4	15.3
Sb	19	14	32	123	17	5.1	5148	3059
La	9.5	17	11	16	12	4.0	1.2	1.2
Ce	18	37	18	35	24	8.6	1.0	0.9
Pr	2.2	4.4	2.1	4.2	2.9	1.0	<0.01	<0.01
Nd	8.0	15.8	8.7	16.9	10.5	4.1	<0.01	<0.01
Sm	1.9	3.7	2.3	4.0	2.5	0.9	<0.01	<0.01
Eu	5.3	0.9	10	2.6	3.8	0.01	2.4	2.5
Gd	2.1	3.8	2.4	4.1	2.6	0.9	<0.01	<0.01
Tb	0.01	0.01	<0.01	<0.01	<0.01	<0.01	<0.01	<0.01
Dy	1.7	3.7	1.7	3.7	2.4	0.8	<0.01	<0.01
Er	0.9	2.0	1.0	2.0	1.3	<0.01	<0.01	<0.01
Yb	0.9	1.8	0.9	1.8	1.2	<0.01	<0.01	<0.01
Hf	1.3	1.0	0.9	1.8	1.2	<0.01	<0.01	<0.01
Ta	0.9	2.0	<0.01	0.8	1.3	<0.01	<0.01	<0.01
W	1.5	1.7	0.9	1.0	1.6	5.1	<0.01	<0.01
Pb	5.3	6.7	5.6	14.6	5.7	14.4	38	1260
Bi	26	6.6	<0.01	4.2	19	0.01	<0.01	1.6
Th	2.0	4.0	2.1	4.3	2.6	1.1	<0.01	<0.01
U	0.8	1.1	0.9	1.3	0.9	0.01	<0.01	<0.01

Hg	0.004	0.02			0.01	0.001	0.1	0.1

Table 2. Concentration of major and trace elements in L3 catenary-bearing Cu, brushes, train wheels, and railways employed in the Barcelona Metro system.

%	Catenary	Brushes	Wheels	Railways*
C	<0.1	95.4	0.5	0.7
H	<0.1	<0.1	<0.1	0.0002
N	<0.1	<0.1	<0.1	0.004
Cu	95.0	0.1	0.1	0.02
Fe	0.9	0.3	98.0	97.8
Mn	0.004	0.0001	0.7	1.1
Si	nm	nm	nm	0.3
mg/kg				
Al	<0.1	0.03	<0.1	11
Ca	<0.1	0.1	<0.1	<0.1
K	<0.1	<0.1	<0.1	<0.1
Mg	<0.1	<0.1	<0.1	<0.1
P	<0.1	<0.1	<0.1	170
S	<0.1	<0.1	<0.1	98
B	<0.1	7.2	26	<0.1
Ti	53	28	9.8	16
V	17	1.0	15	<0.1
Cr	131	22	1173	<0.1
Co	1.4	<0.1	80	<0.1
Ni	54	9.1	782	192
Zn	102	115	6	ns
Ga	<0.1	<0.1	9.2	ns
Ge	<0.1	<0.1	6.6	ns
As	2.9	<0.1	51	ns
Se	1.3	<0.1	<0.1	ns
Sr	3.9	1.7	<0.1	ns
Zr	1.2	<0.1	<0.1	ns
Nb	0.9	<0.1	11	ns
Mo	2.9	2.4	451	ns
Sn	0.9	15	95	ns
Sb	<0.1	4.9	24	ns
Ba	10	28	0.1	ns
W	1.8	1.6	91	ns
Pb	2.4	4.2	<0.1	ns
Hg	0.14	0.01	0.001	ns

*Data supplied by TMB (Metropolitan Transport of Barcelona); nm: not measured; ns: not supplied

Table 3. PM weight-normalised concentrations for OC, EC., major anions, major oxides, and trace elements in F-L3 and S-L9 platforms and corresponding F-L3/S-L9 and PM10/PM2.5 ratios.

	F-L3		S-L9		F-L3 /S-L9		F-L3	S-L9
µg/m3	PM10	PM2.5	PM10	PM2.5	PM10	PM 2.5	PM10/2.5	PM10/2.5

PMx	339	155	100	90	3.4	1.6		
OC	52	33	8	10	6.5	4.1	1.6	0.8
EC	0.3	1.2	4	3	0.1	0.3	0.3	1.3
OC+EC	53	34	13	13	4.1	2.6	1.6	1.0
ws-Cl-	1	0.4	0.7	0.7	1.4	0.6	2.5	1.0
ws-NO3-	0.8	0.2	1.9	0.2	0.4	0.1	4.0	9.5
ws-SO42-	5.1	2.3	5.9	2	0.9	0.4	2.2	3.0
ws-NH4+	0.6	0.3	0.8	0.4	0.8	0.4	2.0	2.0
SO42-	9.6	2.5	6.1	2	1.6	0.4	3.8	3.1
Fe2O3	144	56	41	46	3.5	1.4	2.6	0.9
CO32-	11	5	6	3	1.8	0.8	2.2	2.0
Ca	5	1.8	3	1.2	1.7	0.6	2.8	2.5
Al2O3	3	1.4	1.4	0.7	2.1	1.0	2.1	2.0
Ba	5	2.2	0.03	0.02	167	73.3	2.3	1.5
Mg	2.1	0.9	0.3	0.13	7.0	3.0	2.3	2.3
CuO	2.2	0.8	0.09	0.15	24.4	8.9	2.8	0.6
MnO	1.8	0.7	0.4	0.4	4.5	1.8	2.6	1.0
ZnO	1.4	0.6	0.2	0.13	7.0	3.0	2.3	1.5
Na	0.7	0.3	0.8	0.2	0.9	0.4	2.3	4.0
K	0.6	0.1	0.5	0.08	1.2	0.2	6.0	6.3
TiO2	0.22	0.08	0.08	0.03	2.8	1.0	2.8	2.7
Cr2O3	0.23	0.09	0.06	0.06	3.8	1.5	2.6	1.0
ng/m^3								
Hg	0.1	0.06	0.04	0.04	2.2	1.4	1.6	1.1
Sr	101	44	6	3	16.8	7.3	2.3	2.0
Zr	72	42	6	8	12.0	7.0	1.7	0.8
Mo	76	38	3	3	25.3	12.7	2.0	1.0
Sb	40	27	15	30	2.7	1.8	1.5	0.5
Sn	44	18	5	5	8.8	3.6	2.4	1.0
Ni	34	16	5	6	6.8	3.2	2.1	0.8
As	24	13	3	1.4	8.0	4.3	1.8	2.1
Pb	30	11	6	3	5.0	1.8	2.7	2.0
V	15	7	10	4	1.5	0.7	2.1	2.5
Co	8	3	1.4	1.3	5.7	2.1	2.7	1.1
P	64	3	14	13	4.6	0.2	21.3	1.1
W	4	3	1.1	1	3.6	2.7	1.3	1.1
Li	3.7	1.5	1.5	0.7	2.5	1.0	2.5	2.1
Hf	2.2	1.4	0.1	0.1	22.0	14.0	1.6	1.0
Rb	2.7	1.1	1.6	0.7	1.7	0.7	2.5	2.3
Nb	1.7	0.9	0.5	0.2	3.4	1.8	1.9	2.5
Ge	1.2	0.7	0.3	0.4	4.0	2.3	1.7	0.8
Ga	1.7	0.7	0.5	0.4	3.4	1.4	2.4	1.3
U	0.3	0.4	0.1	0.3	3.0	4.0	0.8	0.3
Y	0.8	0.4	0.3	0.2	2.7	1.3	2.0	1.5
Th	0.7	0.3	0.2	0.3	3.5	1.5	2.3	0.7
Ta	0.3	0.3	0.04	0.04	7.5	7.5	1.0	1.0
Cd	0.4	0.2	0.1	0.1	4.0	2.0	2.0	1.0
Bi	0.6	0.2	0.1	0.1	6.0	2.0	3.0	1.0
Se	0.2	0.02	0.3	0.02	0.7	0.1	10.0	15.0
La	1.53	0.86	0.64	0.31	2.4	1.3	1.8	2.1
Ce	2.46	1.47	0.99	0.55	2.5	1.5	1.7	1.8
Pr	0.23	0.12	0.07	0.02	3.3	1.7	1.9	3.5
Nd	0.88	0.45	0.28	0.16	3.1	1.6	2.0	1.8
Sm	0.21	0.13	0.05	0.05	4.2	2.6	1.6	1.0
Gd	0.18	0.12	0.05	0.04	3.6	2.4	1.5	1.3
Dy	0.2	0.14	0.05	0.06	4.0	2.8	1.4	0.8
Er	0.1	0.06	0.03	0.02	3.3	2.0	1.7	1.5

Table 4. PM weight-normalised concentrations for OC, EC, major anions, major oxides, and trace elements at F-L3 and S-L9 platforms of the Barcelona Metro system, their respective PM10/PM2.5 ratios, and the PM10 F-L3/S-L9 and PM2.5 F-L3/S-L9 ratios.

	F-L3		S-L9		F-L3	S-L9	F-L3/S-L9	
	PM10	PM2.5	PM10	PM2.5	PM10/PM2.5	PM10/PM2.5	PM10	PM2.5
OC	15	21	8.0	11	0.7	0.7	1.9	1.9

EC	0.1	0.8	4.0	3.3	0.1	1.2	<0.1	0.2
OC+EC	16	22	13	14	0.7	0.9	1.2	1.5
ws-Cl^-	0.3	0.3	0.7	0.8	1.1	0.9	0.4	0.3
ws-NO_3^-	0.2	0.1	1.9	0.2	1.8	8.6	0.1	0.6
ws-SO_4^{2-}	1.5	1.5	5.9	2.2	1.0	2.7	0.3	0.7
ws-NH_4^+	0.2	0.2	0.8	0.4	0.9	1.8	0.2	0.4
SO_4^{2-}	2.8	1.6	6.1	2.2	1.8	2.7	0.5	0.7
Fe_2O_3	42	36	41	51	1.2	0.8	1.0	0.7
CO_3^{2-}	3.2	3.2	6.0	3.3	1.0	1.8	0.5	1.0
Ca	1.5	1.2	3.0	1.3	1.3	2.3	0.5	0.9
Al_2O_3	0.9	0.9	1.4	0.8	1.0	1.8	0.6	1.2
Ba	1.5	1.4	0.0	0.0	1.0	1.4	49	64
Mg	0.6	0.6	0.3	0.1	1.1	2.1	2.1	4.0
CuO	0.6	0.5	0.1	0.2	1.3	0.5	7.2	3.1
MnO	0.5	0.5	0.4	0.4	1.2	0.9	1.3	1.0
ZnO	0.4	0.4	0.2	0.1	1.1	1.4	2.1	2.7
Na	0.2	0.2	0.8	0.2	1.1	3.6	0.3	0.9
K	0.2	0.1	0.5	0.1	2.7	5.6	0.4	0.7
TiO_2	0.1	0.1	0.1	0.03	1.3	2.4	0.8	1.5
Cr_2O_3	0.1	0.1	0.1	0.1	1.2	0.9	1.1	0.9
Hg	0.03	0.04	0.04	0.05	0.7	1.0	0.7	0.9
Sr	30	28	6.0	3.3	1.0	1.8	5.0	8.5
Zr	21	27	6.0	8.9	0.8	0.7	3.5	3.0
Mo	22	25	3.0	3.3	0.9	0.9	7.5	7.4
Sb	12	17	15	33	0.7	0.5	0.8	0.5
Sn	13	12	5.0	5.6	1.1	0.9	2.6	2.1
Ni	10	10	5.0	6.7	1.0	0.8	2.0	1.5
As	7.1	8.4	3.0	1.6	0.8	1.9	2.4	5.4
Pb	8.8	7.1	6.0	3.3	1.2	1.8	1.5	2.1
V	4.4	4.5	10	4.4	1.0	2.3	0.4	1.0
Co	2.4	1.9	1.4	1.4	1.2	1.0	1.7	1.3
P	19	1.9	14	14	9.8	1.0	1.3	0.1
W	1.2	1.9	1.1	1.1	0.6	1.0	1.1	1.7
Li	1.1	1.0	1.5	0.8	1.1	1.9	0.7	1.2
Hf	0.6	0.9	0.1	0.1	0.7	0.9	6.5	8.1
Rb	0.8	0.7	1.6	0.8	1.1	2.1	0.5	0.9
Nb	0.5	0.6	0.5	0.2	0.9	2.3	1.0	2.6
Ge	0.4	0.5	0.3	0.4	0.8	0.7	1.2	1.0
Ga	0.5	0.5	0.5	0.4	1.1	1.1	1.0	1.0
U	0.1	0.3	0.1	0.3	0.3	0.3	0.9	0.8
Y	0.2	0.3	0.3	0.2	0.9	1.4	0.8	1.2
Th	0.2	0.2	0.2	0.3	1.1	0.6	1.0	0.6
Ta	0.1	0.2	0.04	0.04	0.5	0.9	2.2	4.4
Cd	0.1	0.1	0.1	0.1	0.9	0.9	1.2	1.2
Bi	0.2	0.1	0.1	0.1	1.4	0.9	1.8	1.2
Se	0.1	0.01	0.3	0.02	4.6	14	0.2	0.6
La	0.5	0.6	0.6	0.3	0.8	1.9	0.7	1.6
Ce	0.7	0.9	1.0	0.6	0.8	1.6	0.7	1.6
Pr	0.1	0.1	0.1	0.02	0.9	3.2	1.0	3.5
Nd	0.3	0.3	0.3	0.2	0.9	1.6	0.9	1.6
Sm	0.1	0.1	0.1	0.1	0.7	0.9	1.2	1.5
Gd	0.1	0.1	0.1	0.04	0.7	1.1	1.1	1.7
Dy	0.1	0.1	0.1	0.1	0.7	0.8	1.2	1.4
Er	0.03	0.04	0.03	0.02	0.8	1.4	1.0	1.7

Table 5. pH and leachable potential of major and trace elements in PM10 and PM2.5 collected at platforms F-L3 and S-L9 of the Barcelona Metro system.

	F-L3		S-L9	
	PM10	PM2.5	PM10	PM2.5
pH	7.3	7.2	6.9	6.8
$\mu g/m^3$				
Al	<0.01	<0.01	<0.01	<0.01

Ca	3.0	1.4	2.3	1.1
Fe	0.1	0.1	0.03	0.1
K	0.5	0.3	0.3	0.2
Mg	1.1	0.5	0.2	0.1
Na	0.7	0.3	0.8	0.3
P	0.01	<0.01	<0.01	<0.01
S	2.0	1.0	2.1	0.9
ng/m^3				
Li	2.3	0.9	0.7	0.3
B	13	5.8	1.9	0.6
Sc	3.2	2.1	1.3	1.1
Ti	2.3	1.5	1.0	0.9
V	0.2	0.03	0.2	<0.01
Cr	0.4	<0.01	0.9	0.1
Mn	53	48	21	38
Co	<0.01	<0.01	<0.01	<0.01
Ni	0.3	0.1	1.1	0.4
Cu	56	30	7.8	12
Zn	9.9	11	25	14
As	11	8.2	0.1	<0.01
Se	0.2	<0.01	0.2	<0.01
Rb	0.9	0.5	0.2	0.2
Sr	36	19	3.9	1.9
Mo	14	8.0	0.3	0.1
Sn	<0.01	<0.01	0.1	<0.01
Sb	8.1	4.2	3.1	1.9
Ba	793	614	8.2	13
Pb	<0.01	<0.01	0.04	<0.01

Table 6. Total content and speciation of As and Sb in selected PM2.5 and PM10 filters from Barcelona Metro platforms F-L3 and S-L9.

Platform	PMx	Filter code	Total As (ng/m3)	Extracted AsIII (ng/m3)	Extracted AsV (ng/m3)	Total extracted As (ng/m3)	Extraction As (%)	AsIII (%)	AsV (%)
S-L9	PM2.5	T364	2.6	0.4	0.3	0.7	25.2	60.0	40.0
	PM10	T306	5.6	0.7	0.3	1.0	17.9	71.4	28.6
	PM10	T267	3.1	1.2	1.8	3.0	97.3	39.1	60.9
Platform	**PMx**	**Filter code**	**Total Sb (ng/m3)**	**Extracted SbIII (ng/m3)**	**Extracted SbV (ng/m3)**	**Total extracted Sb (ng/m3)**	**Extraction Sb (%)**	**SbIII (%)**	**SbV (%)**
F-L3	PM2.5	T368	32	0	8.1	8.1	25.4	0	100
	PM2.5	T318	32	0	5.6	5.6	17.4	0	100
	PM10	T280	50	0	11.0	11.0	21.9	0	100
	PM10	T274	27	0	8.7	8.7	32.0	0	100
S-L9	PM2.5	T364	16	1.6	6.3	7.9	49.2	20.0	80.0
	PM10	T267	12	3.9	5.2	9.2	76.5	42.9	57.1
	PM10	T272	12	2.9	5.5	8.4	69.8	34.4	65.6

FIGURES

Figure 1. Morphology of frontal (a) and lateral (b) metro train brake pads, respectively (top), and sections obtained by diamond disk cutting and polishing (bottom). Two different layers (reddish and dark) are clearly visible in the frontal brake pads (a, bottom).

Figure 2. Appearance of a section of the catenary bearing Cu (a), wheel lathe tailings (b), and brushes (c) analysed in this study.

Figure 3. XRD spectra of the brake lining materials employed in Barcelona Metro trains.

Figure 4. SEM microphotographs and the composition of frontal brake pads used in line 3 Barcelona Metro trains (L3-F); a) general view and limit between reddish and dark layers from L3 brake pads; b) general view of the reddish layer; c and d) Views of the matrix components of the reddish layer; e) General view of the dark layer from L3; f) View of the dark layer matrix.

Figure 5. SEM microphotographs and the composition of lateral brake pads used in Line 3 (L3-L); a) coarse shavings of metallic Fe-particles (generally 200-900µm), sporadic Cu, and aggregates of Ca-Mg-aluminium-silicate cylinders (approximately 100 µm); b) Matrix primarily composed of fine dolomite (5-30 µm), zincite (commonly <5 µm), portlandite, sphalerite, and molybdenite crystals with and Al-rich areas surrounding these minerals; c) Detailed view of zinzite particles.

Figure 6. SEM microphotographs and particle resolved composition of metro brake pads used in Line 9 (L9-L); a) Coarse (mostly around 200µm, but up to 600 µm) and generally rounded particles of metallic-Fe, and sporadically of Cu (containing Zn, Al, and Fe) and Fe-Al particle; b and c) Main components of the brake pad matrix; finer particles (<20µm) of stibnite, barite, periclase, graphite, zincite, calcite, portlandite, and pyrite.

Figure 7. SEM microphotographs presenting the laminar hematite particles collected at the S-L9 platform (a); laminar hematite particles surrounded by a large number of fine particles from the fusion of the catenary and/or steel commonly found in the PM collected at the F-L3 platform (b); single barite crystal and rough Fe particle with fine particles of Ba and Cu (c); and detail of the fusion particles and rough Fe particles with Ba and Cu (d).

Figure 8a. PM10/PM2.5 partitioning and the water soluble and insoluble proportions of As, Hg, Sb, Ba, and Zn in PM10 and PM2.5 for platforms F-L3 and S-L9.

Figure8b. PM10/PM2.5 partitioning and the water soluble/insoluble proportions of Mo, Cu, Cr, Mn, and Ni in PM10 and PM2.5 for platforms F-L3 and S-L9.

FIGURE 1

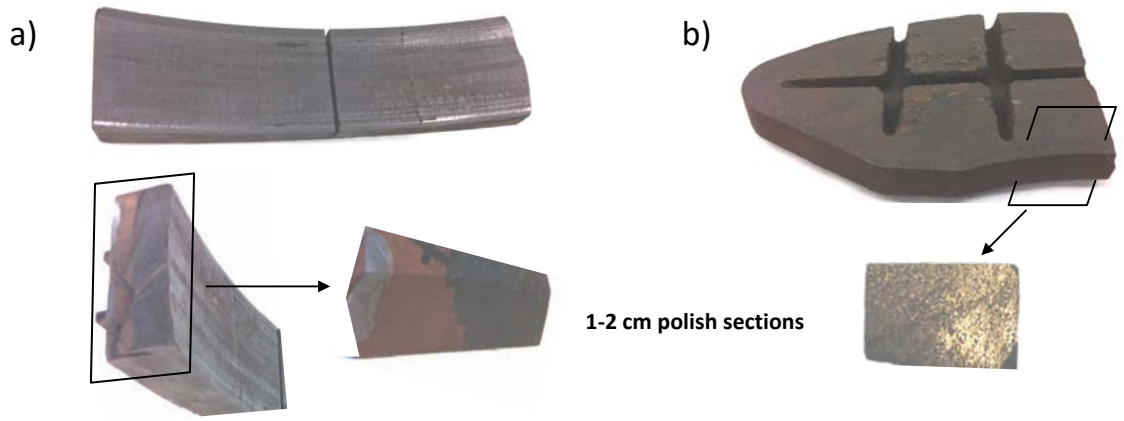

FIGURE 2

FIGURE 3

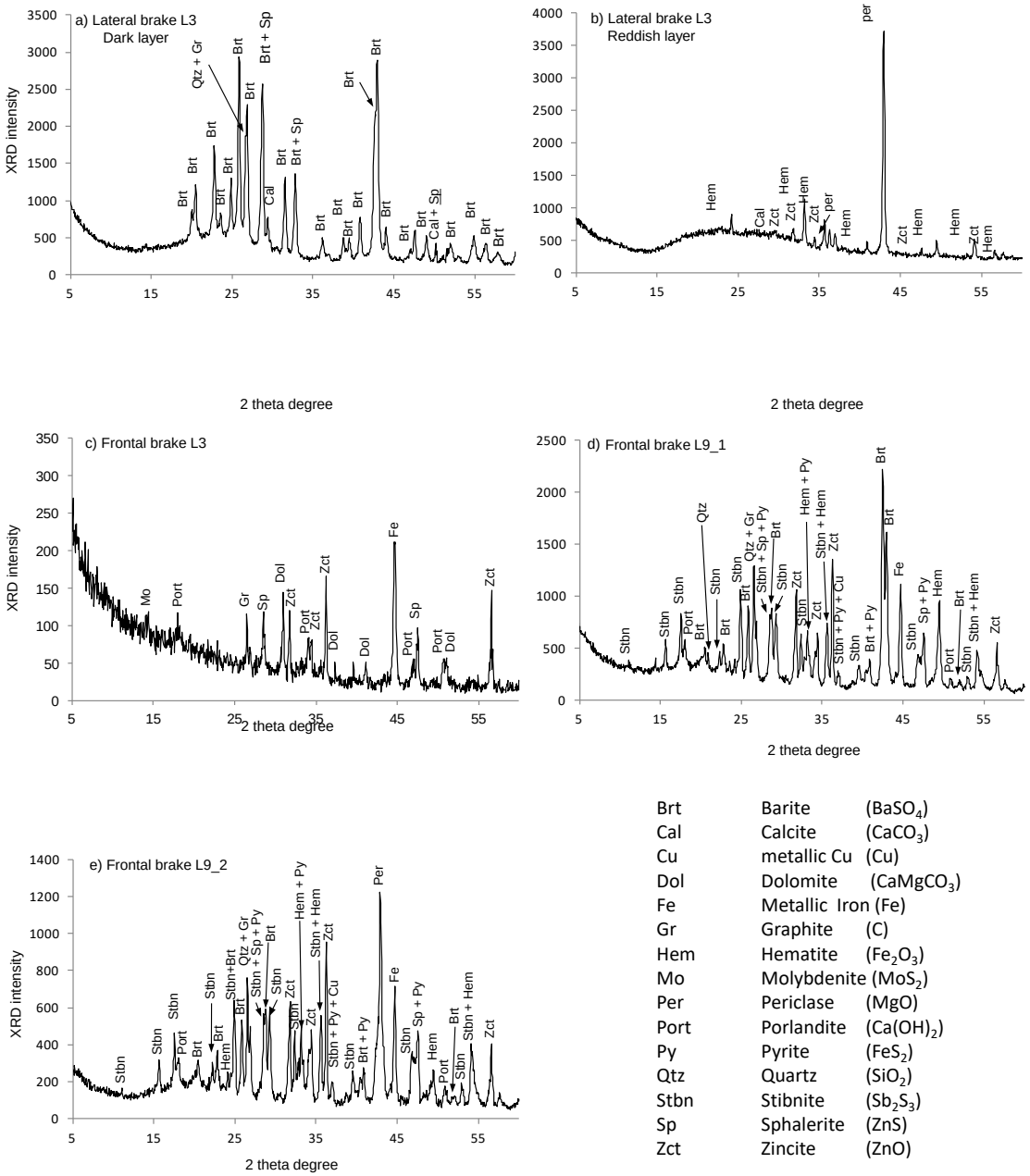

Brt	Barite	($BaSO_4$)
Cal	Calcite	($CaCO_3$)
Cu	metallic Cu	(Cu)
Dol	Dolomite	($CaMgCO_3$)
Fe	Metallic Iron	(Fe)
Gr	Graphite	(C)
Hem	Hematite	(Fe_2O_3)
Mo	Molybdenite	(MoS_2)
Per	Periclase	(MgO)
Port	Porlandite	($Ca(OH)_2$)
Py	Pyrite	(FeS_2)
Qtz	Quartz	(SiO_2)
Stbn	Stibnite	(Sb_2S_3)
Sp	Sphalerite	(ZnS)
Zct	Zincite	(ZnO)

FIGURE 4

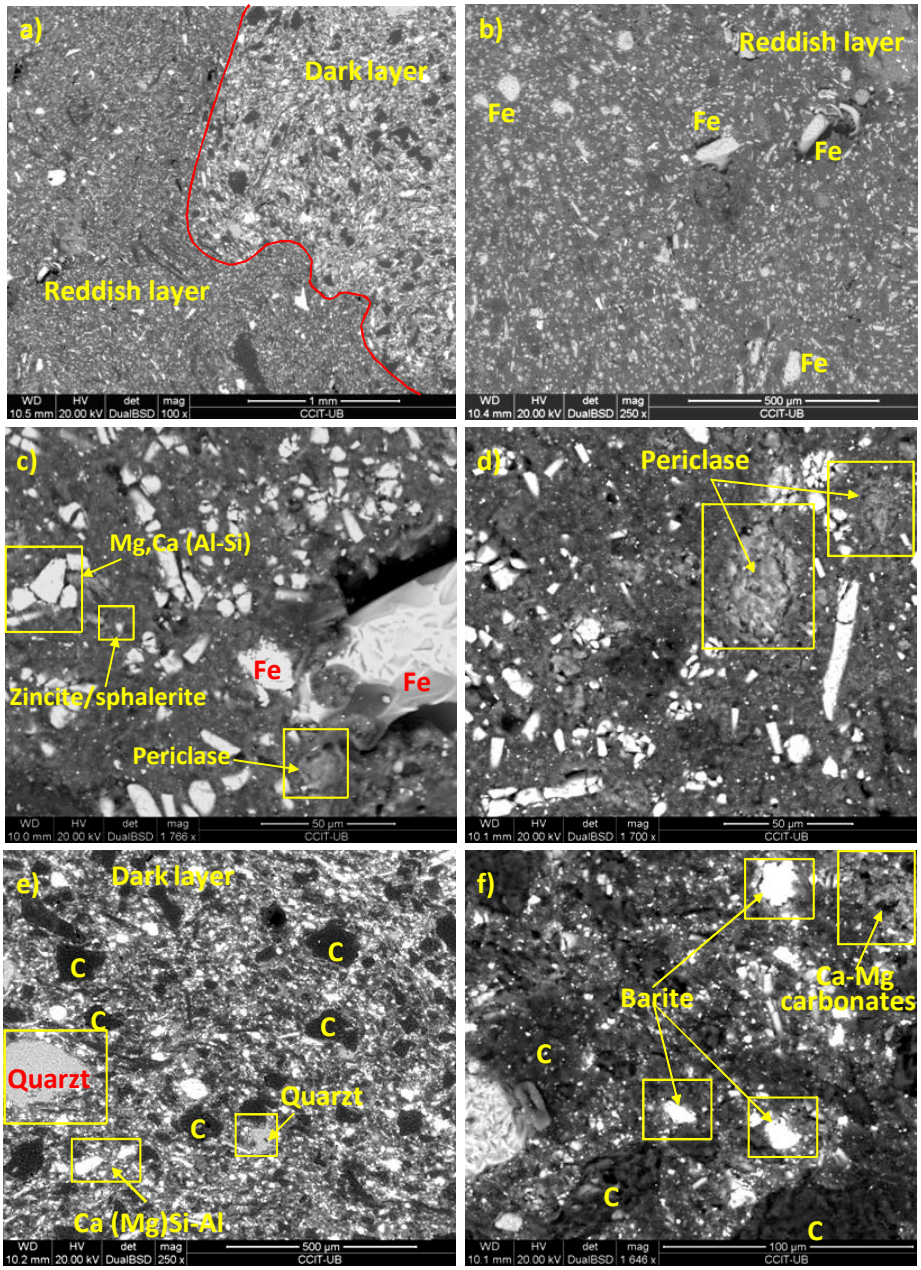
a)
Dark layer
Reddish layer
b)
Reddish layer
Fe
Fe
Fe
Fe
c)
Mg,Ca (Al-Si)
Zincite/sphalerite
Fe
Fe
Periclase
d)
Periclase
e)
Dark layer
C
C
C
C
C
Quarzt
Quarzt
Ca (Mg)Si-Al
f)
Barite
Ca-Mg carbonates
C
C
C

FIGURE 5

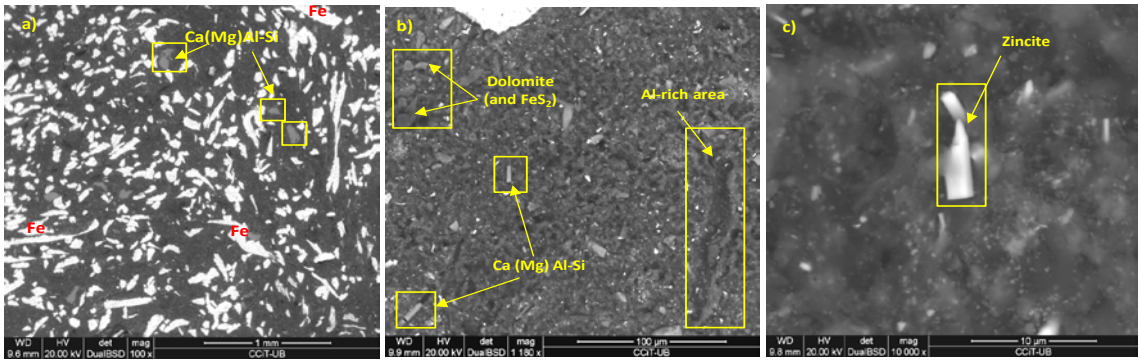
a)
Ca(Mg)Al-Si
Fe
Fe
Fe
b)
Dolomite
(and FeS2)
Al-rich area
Ca (Mg) Al-Si
c)
Zincite

FIGURE 6

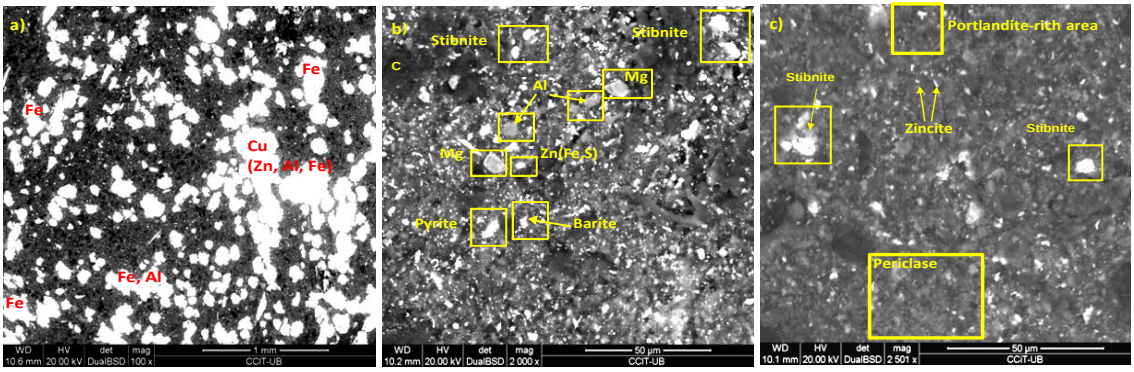

FIGURE 7

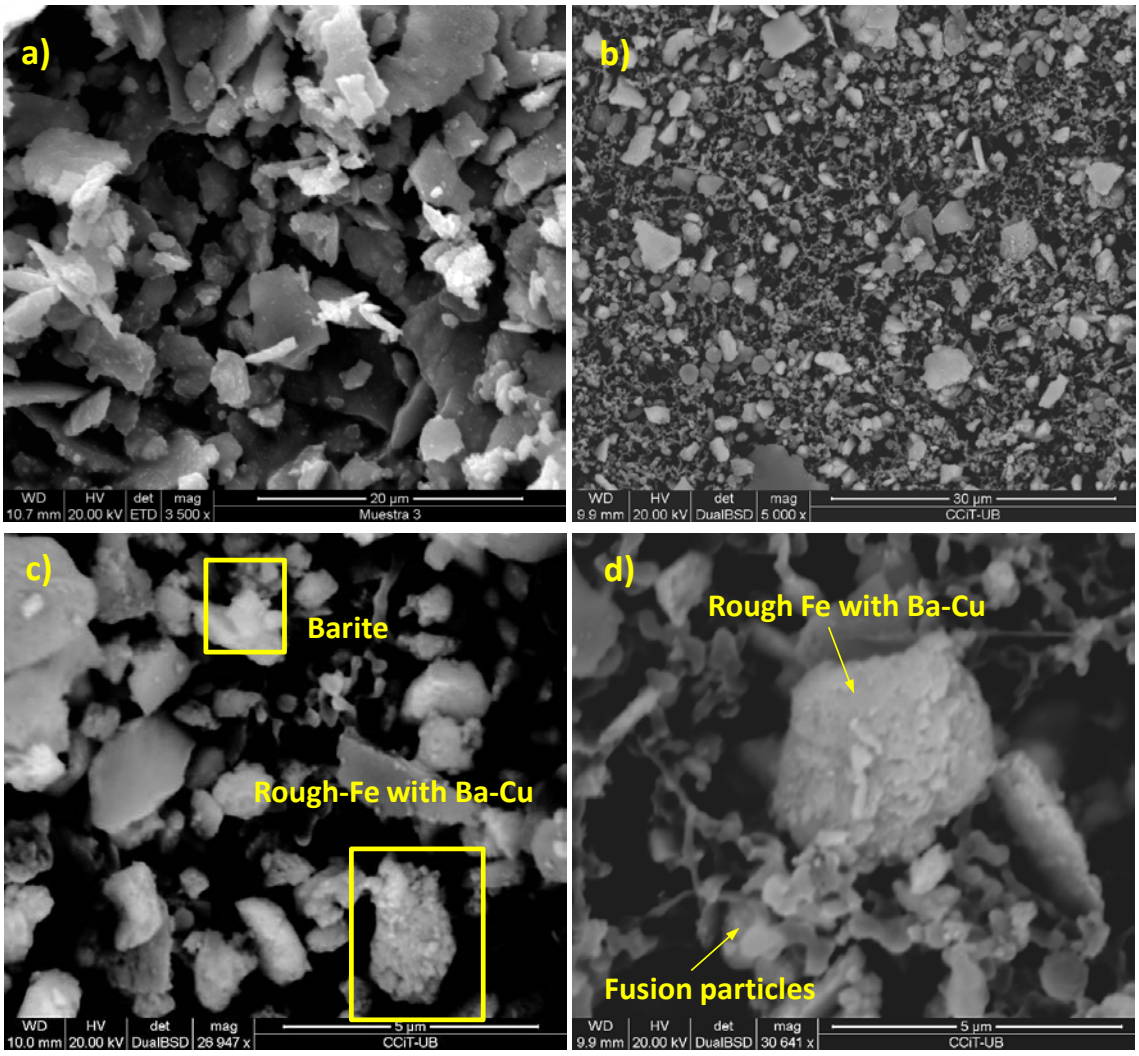

171
172
173

174 FIGURE 8a

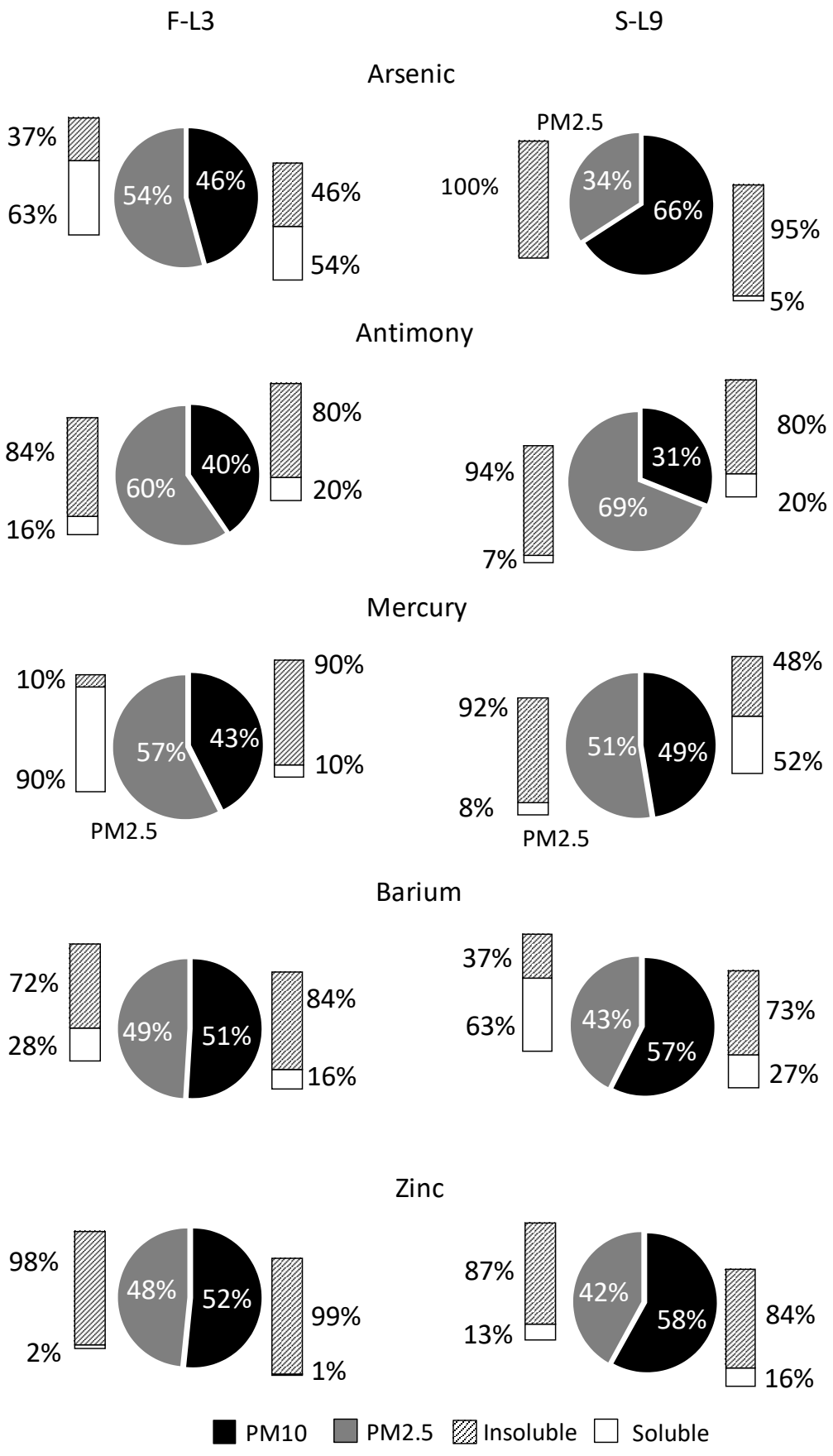
F-L3
S-L9
Arsenic
37%
63%
54%
46%
46%
54%
PM2.5
100%
34%
66%
95%
5%
Antimony
84%
16%
60%
40%
80%
20%
94%
7%
69%
31%
80%
20%
Mercury
10%
90%
57%
43%
90%
10%
PM2.5
92%
8%
51%
49%
48%
52%
PM2.5
Barium
72%
28%
49%
51%
84%
16%
37%
63%
43%
57%
73%
27%
Zinc
98%
2%
48%
52%
99%
1%
87%
13%
42%
58%
84%
16%
PM10
PM2.5
Insoluble
Soluble

Figure 8b

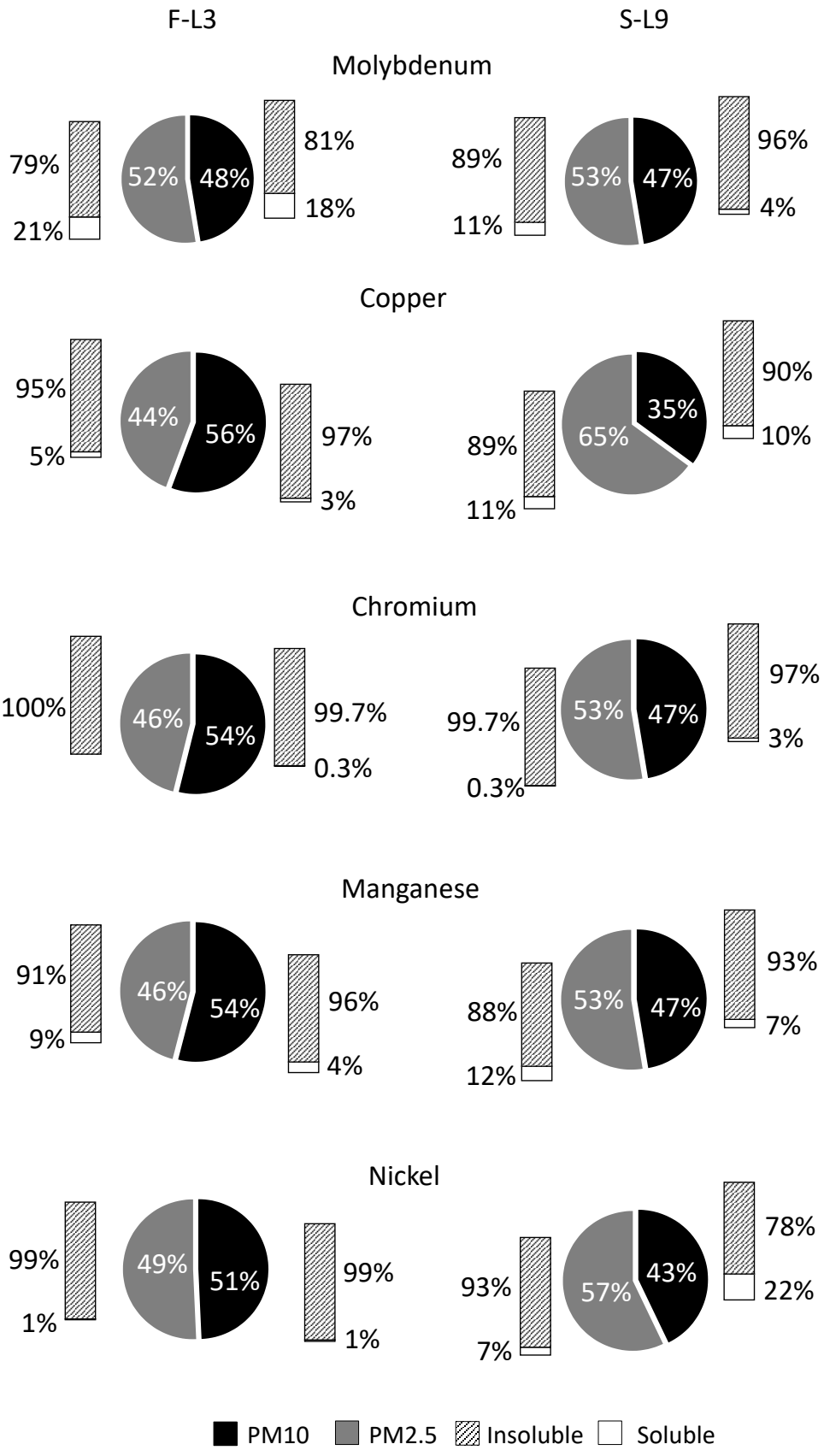
F-L3
S-L9
Molybdenum
79%
21%
52%
48%
81%
18%
89%
11%
53%
47%
96%
4%
Copper
95%
5%
44%
56%
97%
3%
89%
11%
65%
35%
90%
10%
Chromium
100%
46%
54%
99.7%
0.3%
99.7%
0.3%
53%
47%
97%
3%
Manganese
91%
9%
46%
54%
96%
4%
88%
12%
53%
47%
93%
7%
Nickel
99%
1%
49%
51%
99%
1%
93%
7%
57%
43%
78%
22%
PM10
PM2.5
Insoluble
Soluble

177
178

SUPLEMENTARY MATERIAL

S1. L3-FD/L3-FR/L9- concentration ratio for major and trace elements.

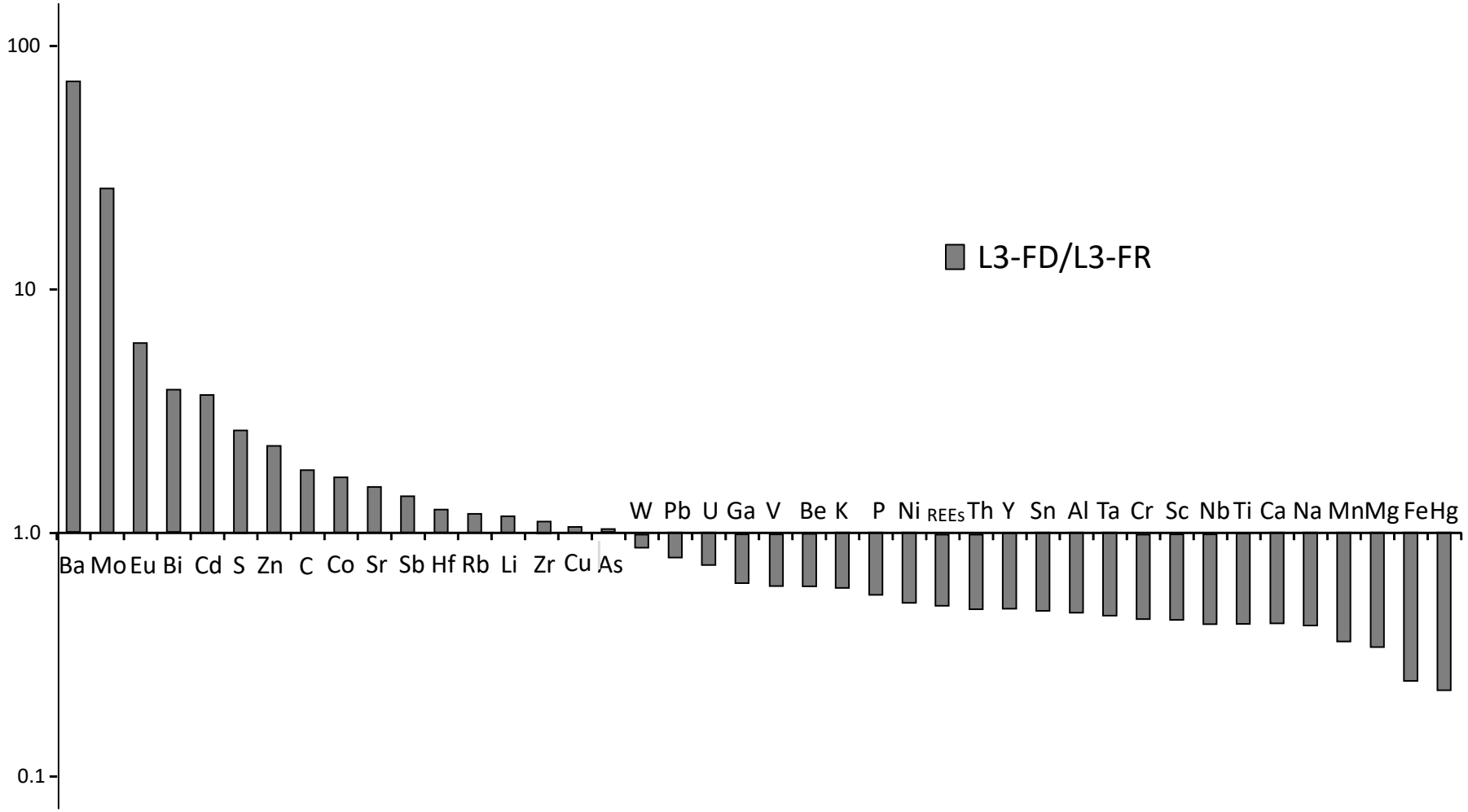

S2. L3-F/L9-L and L3-L/L9-L concentration ratio for major and trace elements.

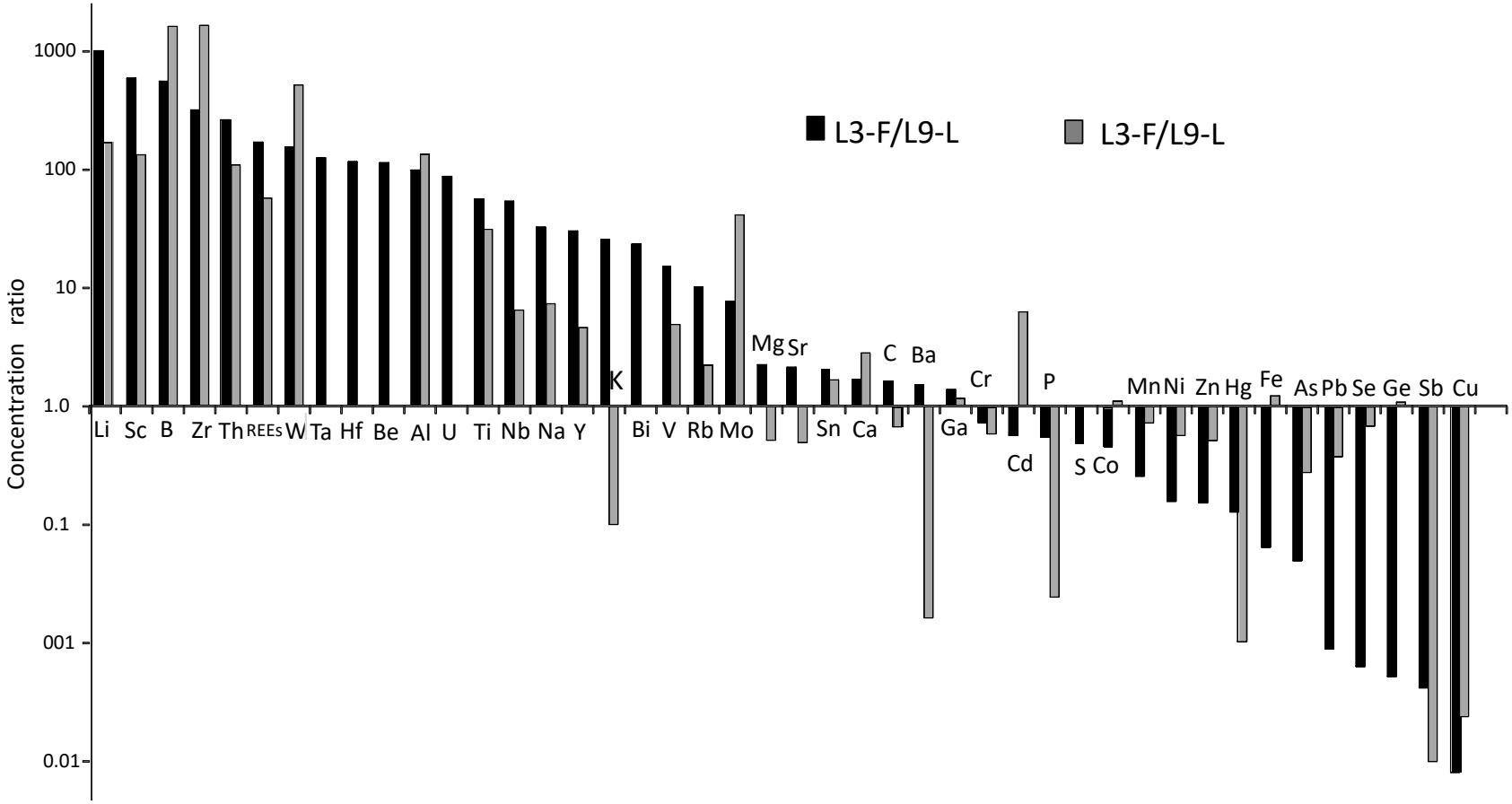

S3. Concentrations of the major and trace elements in the analysed standard 1633b (from two digestion process) and compared with the certified values obtained for R2 and slope of the line between each analysed standard and the certified values. See that the slope values are very close to 1 indicating the close values between analysed and certified values.

%	1633b analysed	1633b analysed	1633b certified
Al	12,7	14,2	14,8
Ca	1,51	1,38	1,47
Fe	7,64	7,26	7,45
K	1,94	1,78	1,89
Mg	0,47	0,47	0,45
Na	0,24	0,17	0,19
P	0,25	0,21	0,25
S	0,18	0,18	0,2
mg/kg			
Li	132,9	134,6	166
Be	12,4	12,6	14
Sc	30,6	35,2	39
Ti	7697,7	7741,5	7517
V	287,3	288,3	296
Cr	170,7	180,1	189
Mn	115,8	120,4	135
Co	44,5	44,7	44,5
Ni	99,1	96,7	125
Cu	106,3	105,9	114
Zn	204,1	202,1	212
Ga	54,1	55,5	61
Ge	15,7	15,6	16
As	130	131	134
Se	10,8	10,9	10,2
Rb	129,8	133	124
Sr	1062,8	1128,6	1069
Y	71,5	75,3	78
Zr	187,8	189,8	202
Nb	23,3	24,2	37
Mo	16,7	20	20
Sn	6,6	7,6	6,6
Sb	6,7	6,8	5,6
Cs	10,2	10,5	10
Ba	722,7	739,2	708
La	80,3	86,6	72
Ce	160,6	184,5	199
Pr	20,6	21,7	19
Nd	86,4	90,6	86
Sm	17,4	18,1	19,1
Eu	4,1	4,2	2,8
Gd	16,1	17,3	17,9
Tb	2,4	2,5	2,4
Dy	15,6	16,3	14,2
Ho	3	3,1	2,7
Er	8,5	8,8	6,6
Tm	1,2	1,2	1,2
Yb	7,4	7,6	7
Lu	0,9	1	1,1
Hf	5,8	6,4	5,7
Ta	2,6	2,6	3,4
W	6,1	6,3	8,6
Tl	6,1	6	5,7
Pb	72,3	69,6	63,4
U	8,2	8,4	8,3
R2	0,9999	0,9999	
Slope	0,9776	0,9709	

S4. Lechable concentrations of major and trace elements from frontal (L3-FD frontal dark layer and L3-FR (frontal reddish layer); and lateral (L3-L) brake pads from F-L3 and S-L9 (L9-L1 and L9-L2).

mg/kg	L3-FD1	L3-FR1	L3-L	L9-L1	L9-L2
pH	11.1	10.4	10.3	10.7	10.7
Al	<0.01	<0.01	<0.01	<0.01	<0.01
Ca	2563	3691	3336	7440	8691
Fe	<0.01	<0.01	<0.01	<0.01	<0.01
K	574	225	<0.01	123	116
Mg	1139	477	41	1566	1115
Na	380	970	63	92	55
P	<0.01	<0.01	<0.01	<0.01	<0.01
S	337	284	755	7845	10039
Si	838	1738	309	50	66
Li	0.01	0.2	0.5	0.1	0.04
B	0.1	0.4	0.5	0.2	0.3
Ti	<0.001	0.01	0.04	<0.001	0.01
V	0.03	0.1	0.2	0.04	0.01
Cr	0.02	0.07	0.05	0.01	0.02
Mn	<0.001	0.01	0.04	<0.001	<0.001
Co	<0.001	<0.001	0.007	<0.001	0.007
Ni	0.1	0.02	0.03	0.1	0.1
Cu	0.1	0.1	0.3	0.1	0.1
Zn	1.4	0.3	0.9	0.1	0.2
Ga	<0.001	<0.001	<0.001	<0.001	<0.001
Ge	<0.001	<0.001	<0.001	<0.001	<0.001
As	0.01	<0.001	<0.001	0.6	0.4
Se	0.02	0.02	0.03	0.03	0.2
Rb	0.04	0.09	0.78	0.05	0.06
Sr	2.0	6.1	1.8	2.0	3.2
Y	<0.001	<0.001	<0.001	<0.001	<0.001
Zr	<0.001	0.02	0.06	0.06	0.04
Nb	<0.001	<0.001	<0.001	<0.001	<0.001
Mo	3.9	5.5	22.9	1.4	0.8
Cd	<0.001	<0.001	0.02	<0.001	<0.001
Sn	0.020	<0.001	0.01	<0.001	<0.001
Sb	3.4	30.0	7.9	1973	2189
Ba	3.2	19	28	6.0	15
Pb	<0.001	<0.001	<0.001	<0.001	<0.001

16 S5. Leachable concentrations of major and trace elements from catenary, train wheels, and brushes.

mg/kg	Catenary	Train wheels	Brushes
Al	<0.01	<0.01	<0.01
Ca	31	22	17
Fe	<0.01	39	<0.01
K	<0.01	<0.01	<0.01
Mg	<0.01	3.6	<0.01
Mn	8.3	6.7	4.9
Na	<0.01	<0.01	<0.01
P	<0.01	<0.01	<0.01
S	<0.01	15	<0.01
Si	<0.01	105.0	<0.01
Li	<0.01	<0.01	<0.01
B	<0.01	<0.01	<0.01
Ti	<0.01	<0.01	<0.01
V	<0.01	<0.01	<0.01
Cr	<0.01	<0.01	<0.01
Mn	8.2	6.5	4.9
Co	<0.01	<0.01	<0.01
Ni	<0.01	0.3	<0.01
Cu	114	22	<0.01
Zn	5.3	1.3	<0.01
Ga	<0.01	<0.01	<0.01
Ge	<0.01	<0.01	<0.01
As	<0.01	<0.01	<0.01
Se	<0.01	<0.01	<0.01
Rb	<0.01	<0.01	<0.01
Sr	0.1	<0.01	<0.01
Y	<0.01	<0.01	<0.01
Zr	<0.01	<0.01	<0.01
Nb	<0.01	<0.01	<0.01
Mo	0.1	0.00	<0.01
Cd	<0.01	<0.01	<0.01
Sn	<0.01	<0.01	<0.01
Sb	1.0	1.1	<0.01
Ba	2.6	1.4	0.3
Hf	<0.01	<0.01	<0.01
Ta	<0.01	<0.01	<0.01
W	<0.01	<0.01	<0.01
Pb	<0.01	<0.01	<0.01

17